Gravity currents in a two-layer stratified ambient: The theory for the steady-state (front condition) and lock-released flows, and experimental confirmations

M. R. Flynn, M. Ungarish, and A. W. Tan

Articles you may be interested in

Gravity currents in a two-layer stratified ambient: The theory for the steady-state (front condition) and lock-released flows, and experimental confirmations

M. R. Flynn,[1,a)] M. Ungarish,[2] and A. W. Tan[1,b)]

[1]*Department of Mechanical Engineering, University of Alberta, Edmonton, Alberta T6G 2G8, Canada*
[2]*Department of Computer Science, Technion, Haifa 32000, Israel*

We consider the propagation of a gravity current of density ρ_c at the bottom of a two-layer stratified ambient in a horizontal channel of height H, in the high-Reynolds number Boussinesq domain. The study emphasizes theoretical-analytical modeling, however, experimental and Navier-Stokes simulation data are also presented and their comparison with theory is discussed. The stratification parameters are $S = (\rho_1 - \rho_2)/(\rho_c - \rho_2)$ where ρ is the fluid density, and $\varphi = h_{1R}/H$ where h_{1R} is the (unperturbed) ambient interface height. Here, 1 and 2 denote, respectively, the lower and upper layer and c denotes the gravity current. The reduced gravity is defined as $g' = (\rho_c/\rho_2 - 1)g$. Rigorous results are obtained for the steady-state analogue of the classical problem of Benjamin [J. Fluid Mech. **31**, 209 (1968)], in which the half-infinite gravity current has thickness h and speed U. We thereby demonstrate that the Froude number $\mathcal{F} = U/(g'h)^{1/2}$ is a function of $a = h/H$, S, and φ. In general, two solutions (or modes) may be realized. Issues of energy dissipation, sub- vs. supercriticality with respect to long internal waves and, more generally, the influence of upstream-propagating disturbances are discussed. For a gravity current released from a lock of height h_0 and length x_0, we derive an approximate shallow-water model and show that the motion is in this case governed by $\Xi = H/h_0$, S, and φ. Although the shallow-water model neglects motion in the ambient layers and ignores the impact of propagation on stratification, the gravity current front speed in the slumping stage is in excellent agreement with measured data. Our theoretical solutions are consistent with previous results (in particular, Holyer and Huppert [J. Fluid Mech. **100**, 739 (1980)] and Tan *et al.* [Environ. Fluid Mech. **11**, 203 (2011)]), but have the advantages of being (i) derived without reliance on adjustable constants and *ad hoc* closures; (ii) applicable to a significantly broader range of dimensionless parameters; and (iii) better assessed by comparison against measured data. The present one-layer shallow-water approximation turns out to be a simple and versatile extension of existing models for homogeneous and linearly stratified ambients, and can be straightforwardly incorporated into the available prediction tools for gravity currents. © *2012 American Institute of Physics*. [doi:10.1063/1.3680260]

I. INTRODUCTION

Pollution discharge into marine environments or the atmosphere must inevitably consider the influence of ambient stratification be it a continuous or discrete function of height. For example, in the case of buoyant plumes rising through a stably stratified medium, one may estimate the maximum rise height and level of neutral buoyancy from the details of the ambient density profile.[1,2] Conversely, in
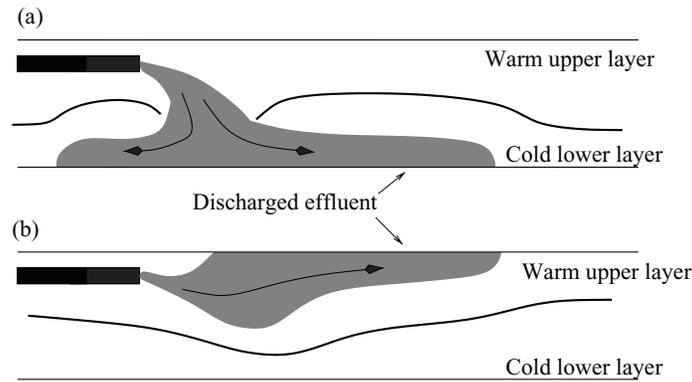

FIG. 1. Effluent discharge in stratified marine environments. (a) Dense effluent and (b) buoyant effluent.

examining the lateral spreading of an intrusive gravity current along a density interface, mimicking say the motion of an effluent along a thermocline, Sutherland and Nault[3] found that the flow may travel unusually long distances at constant speed, but only for particular values of the interface thickness.

The present investigation considers a problem of buoyancy-driven flow that results in predominantly horizontal, rather than vertical, motion. More specifically, and for definitiveness, we shall examine the flow depicted schematically in Figure 1(a), which shows a gravity current propagating at the base of a two-layer stratified ambient. The gravity current density, ρ_c, is assumed to be larger than that of the upper (ρ_2) or lower (ρ_1) ambient layer, however, density differences are small so that the Boussinesq approximation applies. Our study is therefore pertinent to either a dense effluent propagating along a channel floor (Figure 1(a)) or to a light effluent propagating along the underside of a free surface (Figure 1(b)).

Although experimental and numerical data will be presented and discussed in Secs. IV–VI, the major impetus of our study is theoretical-analytical. In this respect, there are two interrelated problems to consider: (i) the idealized steady-state gravity current of height h and speed U, which is the obvious extension of Benjamin's classical solution and (ii) the more practical gravity current produced from rest by lock-release at time $t = 0$ of a fixed volume of dense fluid. The latter problem is time-dependent, but it is expected that results from (i) will provide useful insights (qualitative at least) into the dynamics of the leading domain. The important non-dimensional parameters are $\varphi \equiv h_{1R}/H$, where h_{1R} and H are the undisturbed ambient interface height and channel depth, respectively, and S, a stratification parameter defined as

$$S = \frac{\rho_1 - \rho_2}{\rho_c - \rho_2} , \tag{1.1}$$

which is in the range $0 \leq S \leq 1$ (cf. Eq. (2.2) of Ungarish and Huppert[4]). For the steady-state problem (i), the additional non-dimensional parameter is the height ratio $a \equiv h/H$ of the gravity current to the ambient. Conversely, solutions of the lock-release problem (ii), will depend upon $\Xi \equiv H/h_0$ in which h_0 is the initial depth of the gravity current fluid in the lock.

The steady-state analysis seeks to extend the seminal investigation of Benjamin[5] and thereby derive a relationship of the form

$$\frac{U}{(g'h)^{1/2}} = \mathcal{F}(a, \varphi, S) , \tag{1.2}$$

in which U is the speed of the gravity current (in the laboratory frame in which the unperturbed ambient is stagnant), and

$$g' = (\rho_c/\rho_2 - 1)g \tag{1.3}$$

is the reduced gravity where g denotes gravitational acceleration; the dimensionless $\mathcal{F}$ is usually referred to as a Froude number.

Note that Benjamin considered the simpler (perhaps simplest) problem of gravity current flow through a uniform ambient; correspondingly in his study $\mathcal{F}$ is a function of a alone, and expressible in a closed-form algebraic formula. However, even for that straightforward case some variations in the definitions arise. For instance, it is possible to use $(g'H)^{1/2}$ as the reference speed in Eq. (1.2); but this lacks physical justification, and the so-scaled results become confusing for deep-ambient gravity currents in the limit $a \to 0$. In any case, it is important to recall that $\mathcal{F}$ provides one equation for two unknown properties of the gravity current, U and h. Equation (1.2) does not determine the flow, it is just a necessary constraint on the flow field of the steady gravity current.

When the ambient is inhomogeneous the relationship $\mathcal{F}$ is mathematically more complicated, first of all because more parameters are involved. The physical problem is also more complex. Consider, for example, a linearly stratified ambient fluid whereby $\rho_a(z) = \rho_2 + S(\rho_c - \rho_2)(1 - z/H)$. In the ambient above the gravity current, $h < z < H$, the density and speed are unknown z-dependent functions whose determination is part of the problem. Although a direct analytical solution of the flow field is hopeless, the methodology of Ungarish[6] and White and Helfrich[7] is helpful. First, irrotational solutions of the Euler equations are derived corresponding to a flow in a channel of height H of upstream speed U, which encounters a semi-infinite solid obstacle having in the downstream domain the same constant thickness h as the gravity current. Subsequent replacement of the obstacle with a slug of dense fluid while maintaining the same flow field in the up- and downstream domains of the ambient, subject to the flow-force balance necessary for maintaining a steady state, excludes all but a handful of (eigen-) solutions for $U/(g'h)^{1/2} = \mathcal{F}$. These solutions cannot be expressed in closed analytical form. Multiple solutions are obtained in some domains of the parameter space (mostly for small a and S close to 1). The advantage of this approach is that the solution involves only algebraic equations, it is self-contained and neither requires nor admits adjustable constants. In addition, when $S \to 0$, Benjamin's solution is recovered. We expect that the same procedure will provide reliable insights here. Accordingly, we will develop the $\mathcal{F}$ relationship for the present two-layer stratification. This relationship will be subsequently compared against analogue experimental and Navier-Stokes simulation data obtained as a part of the present investigation.

Steady-state gravity currents are, in general, dissipative: in a frame of reference moving with the front, there is a disparity of energy fluxes far up- and downstream. Only solutions in which the energy is conserved or decreases are feasible, and this yields the restriction $a \le a_{\max}$, where $a_{\max}$ corresponds to a non-dissipative gravity current. For Benjamin's classical result $a_{\max} = \frac{1}{2}$; ambient stratification decreases this value and may also restrict the feasible domain from below as discussed in Sec. V. Note that the solutions of Benjamin[5] and Ungarish[6] do not make any *a priori* assumption concerning the magnitude of dissipation. Rather, this is an outcome of their respective analyses.

The lock-release problem is more practical than that of the steady-state gravity current, certainly from the perspective of laboratory experiments. However, because the lock-release flow is governed by partial differential, rather than algebraic, equations, the solution is, in general, more difficult to ascertain. The advantage of examining the lock-release configuration regards validation: it is relatively easy to obtain accurate laboratory and Navier-Stokes simulation data, in particular, for the speed of propagation. There are, moreover, both experimental and theoretical evidences that during the initial (or slumping) stage of propagation, the leading part of the gravity current resembles a steady-state current. This facilitates comparisons with and assessments of the steady-state results. Indeed, a large part of the present investigation is concerned with the lock-release problem for general Ξ (ratio of ambient to lock heights). Accordingly, we present a shallow-water (SW) model and closed analytical solutions for the speed of propagation in the slumping stage. To our knowledge, such a formulation has not been published before. Second, we show laboratory and Navier-Stokes simulation results which are used for comparisons with the analytical predictions for both the steady-state and lock-released problems.

A forerunner of the present analysis is the investigation of Holyer and Huppert.[8] The steady-state gravity current problem considered in that work is the same as examined here. (Holyer and Huppert[8] separately studied the steady propagation of an *interfacial* gravity current in a two-layer stratified ambient. We do not address this topic here, but rather refer the interested reader to the discussion of Ungarish,[9] Flynn and Linden,[10] and Ungarish.[11]) There are, however, differences in the solution. Holyer and Huppert[8] attempted to identify the steady state with the lock-release problem. This was

achieved by making recourse to some restrictive assumptions concerning the nature and magnitude of the energy dissipation, which are difficult to justify. The present solution has the benefit of various pieces of knowledge that have accumulated in the three decades since the publication of Holyer and Huppert's paper. We are now able to derive a solution that does not require these assumptions. Therefore, in our opinion, the present analysis constitutes a more reliable extension of Benjamin's result and a more versatile formulation and solution of the lock-release problem. A second closely related previous investigation is that of Tan *et al.*[12, 13] However, that study covers only the special case of full-depth lock-release, $\Xi = 1$, and here we consider the general case.

To summarize, the present investigation contains novel contributions and significant extensions concerning the theory of both the steady-state and lock-released gravity currents in a two-layer stratified ambient. This is expected to close gaps of knowledge, enhance understanding, and provide a simple predictive tool for these flows.

The rest of the paper is organized as follows: the experimental apparatus and procedure are reviewed in Sec. II. Experimental results are confirmed by comparison against analogue numerical simulations. The numerical code is described in Sec. III and a qualitative comparison between experimental and numerical data is given thereafter in Sec. IV. In Sec. V we consider, by suitable adaptation of Benjamin,[5] Ungarish,[6] and White and Helfrich,[7] the steady propagation of a dense gravity current through a two-layer ambient. Theoretical results are compared against laboratory data. We then present in Sec. VI a simplified shallow-water model, which admits realistic initial/boundary conditions and time-dependent solutions. Model predictions are corroborated by extensive comparison with measured results. Finally, a series of conclusions is provided in Sec. VII.

II. EXPERIMENTAL PROCEDURE

Experiments were performed in a glass tank having the following dimensions: 227.5 cm long by 25.0 cm wide by 30.0 cm tall. A vertical barrier made of plastic served as the lock gate; it was placed at a distance $\ell = 32.4 \pm 0.1$ cm from the left end-wall. (By comparison, the fluid depth, H, was fixed at 20.0 ± 0.1 cm.) The tank was backlight using an electric vinyl light-sheet and experimental images were recorded at either 4 or 8 frames/s using a pair of LaVision GmbH Imager 3 12-bit cameras with 35 mm Nikon AF Nikkor lenses placed ∼4.25 m in front of the tank.

Fluid densities were adjusted by addition of salt (sodium chloride) and were measured using an Anton Paar DMA 38 densitometer having an accuracy of 5×10^{-4} g/cm^3. Although ρ_1 and ρ_c varied, respectively, between 0.9987 g/cm^3 and 1.0446 g/cm^3 and 1.0217 g/cm^3 and 1.0962 g/cm^3, a typical experiment had a gravity current density of $\rho_c \simeq 1.04$ g/cm^3 (see Tan,[14] Appendix F for further details). Density contrasts were always small enough so that the stratified fluid was Boussinesq.

For the full-depth lock-release experiments ($\Xi = 1$), we first filled the tank with dyed tap water ($\rho_2 \simeq 0.9982$ g/cm^3) to a depth h_{2R}. Salt water having a density ρ_1 was then trickled into the tank through a nozzle placed ∼4 mm above the floor. The nozzle was foam-covered to minimize interfacial mixing during the filling process. Tank filling continued (and the supply flow rate gradually increased) until the lower layer depth was h_{1R}. Thereafter, the lock gate was lowered into the tank and more dye (food coloring) and salt were added to the lock region. After manually mixing the lock fluid, the gate, which was guided by a pair of vertical sliders, was smoothly removed from the tank resulting in a gravity current flow.

Partial-depth lock-release experiments with $\Xi > 1$ followed a slightly more involved procedure. When $h_0 < h_{1R}$, the ambient layers were established as described above. After lowering the lock gate, however, fluid from the lower layer of the lock region was drained through a pipe placed at the bottom of the tank. Simultaneously, fluid of density ρ_2 was allowed to flow into the lock, without mixing, through a pair of small holes in the lock gate located at heights of approximately 17.5 cm and 20.0 cm. A significant hydrostatic pressure difference between the lock and ambient regions was thereby avoided. This difference might have otherwise caused leakage across the imperfect seals of the lock gate. Siphoning was terminated once the desired volume of fluid of density ρ_1 had been removed. Salt water of density ρ_c premixed with dye was then slowly added to the lock region through the foam-covered nozzle thereby causing fluid of density ρ_2 to concurrently flow out of the lock region through the aforementioned holes in the gate. Fluid addition continued until the

combined height, H, of the fluids to either side of the gate reached 20.0 ± 0.1 cm, or, equivalently, the ambient interface height reached the same elevation outside and inside the lock.

When $h_{1R} \leq h_0 < H$, the ambient layers were established as described above except that the lighter ambient layer of density ρ_2 was overfilled to a height of $h_{2R} + \Delta H$. After the lock gate was lowered and food coloring and salt were mixed into the lock, lock fluid was then siphoned from the bottom while fluid of density ρ_2 simultaneously flowed into the lock, this time through the upper hole only. Siphoning continued until fluid of density ρ_c spanned a height h_0 inside the lock. The parameter ΔH was chosen so that the total fluid depth then equalled the desired value, namely, 20.0 ± 0.1 cm.

The front speed was measured by evaluating the position of the leading edge of the gravity current through a sequence of images. Two methods were employed to track the position of the front: (i) manual selection of the leading edge for each image; and, more preferably, (ii) using the built-in MATLAB function `normxcorr2`. The height, h, of the gravity current was obtained by measuring the vertical position of the gravity current crest relative to the bottom surface and corresponds to an average value over a significant fraction of the slumping phase. Due, however, to the turbulent mixing and large-scale structures behind the front, this parameter was difficult to measure and thus has a large associated experimental uncertainty. Easier to measure was the initial height, h_0, of the gravity current fluid, which was determined prior to the initiation of the experiment using a conductivity probe (Precision and Measurement Engineering, MSCTI) mounted to a computer controlled traverse (Velmex, X-Slide). The relationship between voltage and density was linear and was verified using stock solutions of known density.

III. NUMERICAL SIMULATIONS

The purpose of the numerical simulations is to provide verification, such as it is required, and extension of our laboratory data. The front speed is again the measured quantity of primary interest. Details of the DNS algorithm (Diablo) used to simulate the flows described in Sec. II have been chronicled at length in related publications.[12, 15] Only the essential details will be recounted here.

In its present implementation, the algorithm solves, using primitive variables, the two-dimensional Navier-Stokes equations by employing a spectral and finite-difference decomposition, respectively, in the horizontal (x) and vertical (z) directions. No slip conditions are applied along the horizontal boundaries $z = 0$ and $z = H$. The fluid density, ρ, which is dynamically coupled to $\mathbf{u} = (u, \, w)$, is solved via

$$\frac{\mathrm{D}\rho}{\mathrm{D}t} = \frac{\nu}{\mathrm{Sc}} \nabla^2 \rho \,, \tag{3.1}$$

where $\nu = 0.01$ cm^2/s is the kinematic viscosity. Consistent with Härtel *et al.*[16] and others, the Schmidt number is chosen as Sc $= 1$.

Time is evolved using a third-order Runge-Kutta-Wray algorithm and a Crank-Nicholson scheme. As with Tan *et al.*,[12] we typically select $\Delta t = 5 \times 10^{-3}$ s, $t_{\max} = 62.5$ s, $\Delta x = 0.195$ cm, $L = 400.0$ cm, $\Delta z = 0.078$ cm, $H = 20.0$ cm, and a maximum density difference of $\rho_c - \rho_2 = 2 \times 10^{-2}$ g/cm^3. Here, L denotes the length of the numerical domain. Different values for the density ratio S are recovered by varying ρ_1 between $\rho_c = 1.02$ g/cm^3 and $\rho_2 = 1.00$ g/cm^3. As summarized in Figure 2, a selected number of simulations were run at higher Reynolds number for which $\Delta t = 2.5 \times 10^{-3}$ s, $\Delta x = 0.111$ cm, and $\rho_c - \rho_2 = 3.39 \times 10^{-2}$ g/cm^3 or $\rho_c - \rho_2 = 3.70 \times 10^{-2}$ g/cm^3. In these higher-Re numerical simulations, $L = 227.5$ cm corresponding to the length of the glass tank described in Sec. II. In all cases, and as with the post-processing of our laboratory data, estimates of the front speed follow from tracking the front position in time.

IV. COMPARISON BETWEEN EXPERIMENTS AND NUMERICAL SIMULATIONS

Figure 2 contrasts snapshot images of experimental (panels (a) and (c)) and numerical (panels (b) and (d)) data. In panels (a) and (b), $\varphi = 0.38 \pm 0.01$, $\Xi = 2.22 \pm 0.10$, and $S = 0.746 \pm 0.047$ ($\pm$ is included to indicate the associated experimental error). Images are shown at
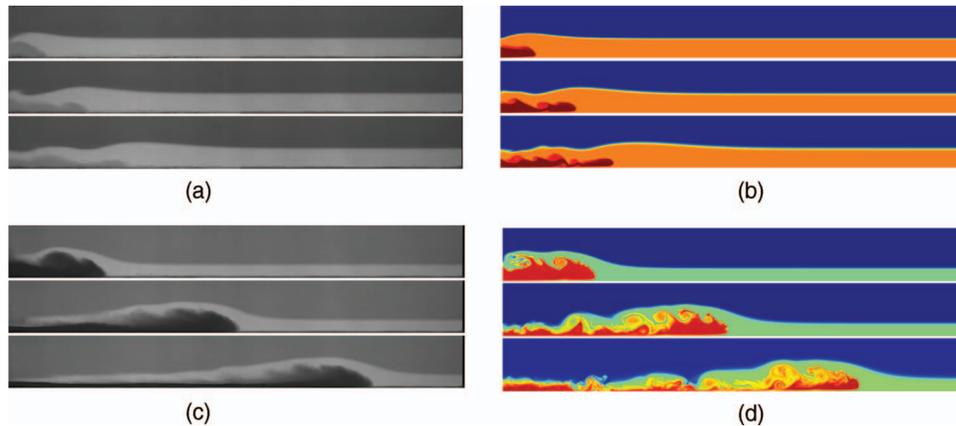
FIG. 2. (Color online) Flow evolution in a complementary pair of experiments (panels (a) and (c)) and numerical simulations (panels (b) and (d)). In the top and bottom row, respectively, images measure 176 cm × 20 cm and 178 cm × 20 cm. Further experimental and numerical parameters are summarized in the text.

$t(g'h_0)^{1/2}/h_0 = 5.02, 10.03$, and 15.06 where $g' = 36.3$ cm/s^2 corresponding to a Reynolds number, based on h_0, of Re $= 16.5 \times 10^3$. Conversely, in panels (c) and (d), $\varphi = 0.25 \pm 0.01$, $\Xi = 1.39 \pm 0.04$, and $S = 0.511 \pm 0.045$. Images are shown at $t(g'h_0)^{1/2}/h_0 = 5.69, 13.30$, and 20.89 where $g' = 33.3$ cm/s^2 corresponding to Re $= 31.2 \times 10^3$. In both cases, fluid densities in the numerical simulations are chosen to match those from the analogue experimental runs.

The correlation between image pairs is encouraging: in each case, generally strong agreement is noted when comparing the front position and the ambient interface shape. Because the DNS algorithm is two-dimensional, one observes in the numerical images much more pronounced vortices in the lee of the front. By comparison, these vortices are rapidly broken down by spanwise instabilities in the real three-dimensional flow. Correspondingly, we see in panel (d), in particular, a series of abrupt deflections to the ambient interface well behind the gravity current head, which are not evident in the experimental images of panel (c). Fortunately, given the aims of the present investigation, such observations are largely moot: the (constant) front speed, U, is unaffected by the coherence of the trailing vortices[17] and their associated perturbations to the ambient interface. Indeed we will show in Figure 11 that there is little difference between the front speeds measured experimentally and those determined from the numerical simulations.

V. THE STEADY-STATE CURRENT AND $\mathcal{F}$ RESULTS

A. Formulation

We start our analysis with a related simpler problem: the steady, stratified flow over a semi-infinite obstacle of height $h = aH$, depicted schematically in Figure 3(a). A solution of this problem is reported in Baines;[18] below, we review the essential features of Baines's solution for the sake of completeness and for the point of comparison to the equations in the subsequent analysis. We assume irrotational flow of an ideal, stress-free fluid. Far up- and downstream of the leading edge, O, of the obstacle, the speed is horizontal and piecewise z-independent. The pressure in these domains is hydrostatic according to $\partial P/\partial z = -\rho_i g$ ($i = 1, 2$). For prescribed upstream (right-hand side) flow conditions, the objective is to determine the corresponding conditions in the downstream parallel flow domain, i.e., h_{1L}, h_{2L}, u_1, and u_2.

Mass conservation applied to the lower and upper ambient layers indicates that

$$U\varphi = u_1\chi\,, \qquad \text{and} \qquad U(1-\varphi) = u_2(1-a-\chi)\,, \tag{5.1}$$

respectively, where $\chi \equiv h_{1L}/H$. These results allow us to eliminate the layer velocities u_1 and u_2 from subsequent equations.
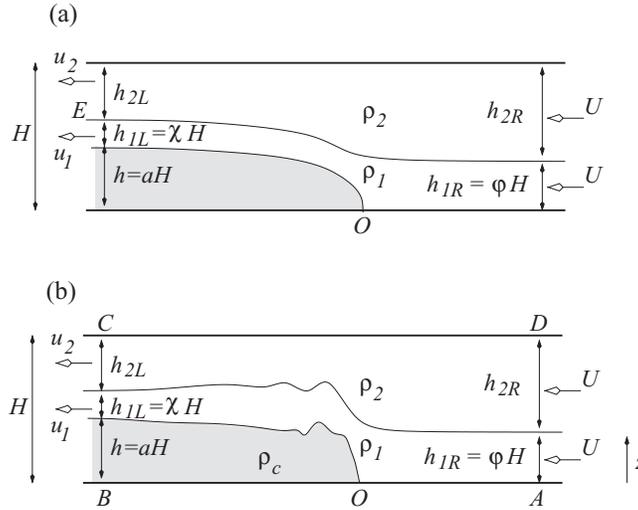
FIG. 3. Definition sketch of (a) steady two-layer flow over a semi-infinite solid obstacle; and (b) a steady, dense gravity current in a two-layer stratified ambient in which the reference frame moves at the front speed, U.

Because the flow is ideal, Bernoulli's equation may be applied in the lower and upper ambient layers. For this purpose, it is convenient to use the reduced pressure $p = P + \rho_2 g z$ and to specify $p = 0$ in the unperturbed upper layer of the ambient (at the right in Figure 3(a)). In addition, the pressure is continuous at the interface between the layers, which is also a streamline. Let E be a point on the downstream horizontal interface, and denote by p_E the pressure there. We obtain for the lower layer

$$\tfrac{1}{2}\rho_1 U^2 \left[1 - (\varphi/\chi)^2\right] = p_E + \rho_2 g' S H (1 + \chi - \varphi), \tag{5.2}$$

and for the upper layer

$$\tfrac{1}{2}\rho_2 U^2 \left[1 - \left(\frac{1-\varphi}{1-a-\chi}\right)^2\right] = p_E. \tag{5.3}$$

We eliminate p_E from Eqs. (5.2) and (5.3), invoke the Boussinesq assumption ($\rho_1 \approx \rho_2$), and the definition $\mathcal{F} = U/(g'h)^{1/2}$, and thereby obtain the dimensionless relationship

$$S\left(\frac{a + \chi - \varphi}{a}\right) = \tfrac{1}{2}\mathcal{F}^2 \left[\left(\frac{1-\varphi}{1-a-\chi}\right)^2 - \left(\frac{\varphi}{\chi}\right)^2\right] \tag{5.4}$$

(cf. (3.6.4b) of Baines[18]). Provided the upstream flow conditions, S, φ, and $\mathcal{F}$, and the obstacle height, $a = h/H$, are given, Eq. (5.4) closes the solution: it admits a solution for χ, from which the downstream layer depths, i.e., $h_{1L} = \chi H$ and $h_{2L} = H - h - h_{1L} = H(1 - a - \chi)$, can be determined. It is then straightforward to compute u_1 and u_2 from Eq. (5.1). Attention is, of course, restricted to physical solutions with positive u_i and h_{iL}.

Now we switch from flow over a solid obstacle to the gravity current problem. Graphically, we replace the shaded region of Figure 3(a) with the slug of fluid of density $\rho_c \geq \rho_1$ shown schematically in Figure 3(b). In a frame moving with the gravity current, O is a stagnation point and the pressure there is $\tfrac{1}{2}\rho_1 U^2 + C$. Inside the slug the pressure is hydrostatic, $P = \tfrac{1}{2}\rho_1 U^2 + C - \rho_c g z$, and there is again pressure continuity at the interface $z = h$.

The first major difference with the solid obstacle solution is that now $\mathcal{F}$ and a cannot be specified independent of one another. To maintain a steady state it is necessary to balance the flow forces on the boundaries of a pertinent control volume about the gravity current head. Our control volume is bounded by the vertical line segments AD and BC of Figure 3(b), and by the horizontal line segments $z = 0$, H. Because there are no external horizontal forces applied to this control volume, a steady

state (zero acceleration) requires that

$$\int_A^D (P + \rho u^2)\mathrm{d}z = \int_B^C (P + \rho u^2)\mathrm{d}z \,, \tag{5.5}$$

where P, ρ, and u denote, respectively, the fluid pressure, density, and velocity. The vertical coordinate, z, is defined in Figure 3(b). Using the hydrostatic pressures in the gravity current and ambient and eliminating u by Eq. (5.1), Eq. (5.5) may be written in dimensionless form as

$$\mathcal{F}^2 a \left[\frac{1}{2} - \frac{\varphi^2}{\chi} - \frac{(1-\varphi)^2}{1-a-\chi} \right] = S \left[\varphi \left(1 - \tfrac{1}{2}\varphi\right) - \chi \left(1 - \tfrac{1}{2}\chi - a\right) \right] + \tfrac{1}{2}a(a-2) \tag{5.6}$$

in which $\mathcal{F}$ is given by Eq. (1.2) (cf. Eq. (2.6) of Holyer and Huppert[8] and Eq. (2.5) of Tan *et al.*[12]).

Equations (5.4) and (5.6) complete the solution of the steady-state gravity current in the sense of Benjamin's analysis. Given the height of the channel and the gravity current (which define a), and the stratification conditions of the far-upstream ambient (in particular, the dimensionless parameters S and φ), we solve (numerically) systems (5.4) and (5.6) for χ and $\mathcal{F}$. A simple analytical result for $\mathcal{F}$ analogous to the well-known $[(2-a)(1-a)/(1+a)]^{1/2}$ of Benjamin[5] seems unattainable, however this is rather a technical detail; the extensions concerning a linearly stratified ambient[6,7] also require a numerical calculation of $\mathcal{F}$ in the final stage.

B. Rate of dissipation and head loss

The second major difference between the flow of the ambient over a solid obstacle and the flow field of the combined gravity current-ambient system concerns energy dissipation. While the solid obstacle is able to passively sustain the vertical force due to the pressure distribution of the ideal flow of the ambient, the slug of fluid of density ρ_c is governed by an internal pressure distribution that must be taken into consideration. This contribution introduces the effects called "dissipation" and "head loss," and imposes a limitation on the range of validity of $\mathcal{F}$ obtained by the aforementioned calculation. (In Benjamin's classical case this is the well-known $a \leq \frac{1}{2}$ restriction.)

The rate of dissipation is the difference between the out- and ingoing energy flux with respect to the control volume. In dimensional form this reads[19]

$$\dot{\mathcal{D}} = \int_A^D \left[(P + \tfrac{1}{2}\rho u^2 + \rho g z) \right] u \, \mathrm{d}z - \int_B^C \left[(P + \tfrac{1}{2}\rho u^2 + \rho g z) \right] u \, \mathrm{d}z \,. \tag{5.7}$$

Evaluating the above integrals and scaling with $\rho_2 h(g'h)^{3/2}$, the *dimensionless* rate of dissipation is expressed as

$$\dot{\mathcal{D}} = \frac{\mathcal{F}}{a} \left\{ 1 - S \left[\varphi + \frac{1}{a}(1-\varphi)(\varphi-\chi) \right] - \tfrac{1}{2}\mathcal{F}^2 \left[\frac{\varphi^3}{\chi^2} + \frac{(1-\varphi)^3}{(1-\chi-a)^2} \right] \right\} \,, \tag{5.8}$$

or, more simply,

$$\dot{\mathcal{D}} = \frac{\mathcal{F}}{a} \left[1 - S - \tfrac{1}{2}\mathcal{F}^2 \left(\frac{\varphi}{\chi} \right)^2 \right] \,, \tag{5.9}$$

where Eq. (5.4) has been applied in deriving the latter expression. The quantity $\dot{\mathcal{D}}$ is calculated numerically for values of $\mathcal{F}$ and χ that satisfy the steady-state conditions of continuity and flow-force balance; see Figures 4–6. This is like in Benjamin's solution, although, again, no analytical expression is available. If $\dot{\mathcal{D}} = 0$ the flow is free of dissipation; this energy-conserving solution is realized for certain values of a. In Benjamin's solution, $\dot{\mathcal{D}} = 0$ occurs for $a = a_{\max} = \frac{1}{2}$ only; in the present stratified case there is, in general, another value of a, $a_{\min} < a_{\max}$, where the solution also has zero dissipation. This observation is consistent with the findings of Holyer and Huppert;[8] details will be presented later. Currents with $\dot{\mathcal{D}} < 0$ are physically unacceptable because $\dot{\mathcal{D}} < 0$ implies the existence of an energy source inside the control volume. By contrast, gravity currents with $\dot{\mathcal{D}} \geq 0$ are realizable. As explained by Benjamin,[5] $\dot{D} > 0$ indicates that some shear, and perhaps turbulence, is present in the domain about the head of the gravity current (as indicated schematically in
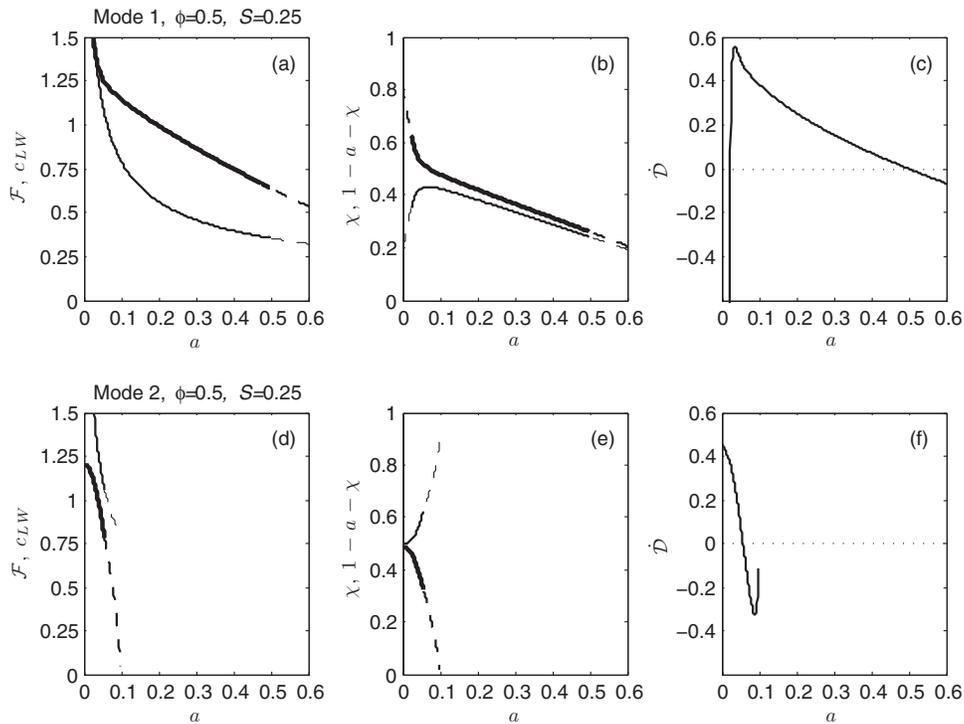
FIG. 4. Solution to Eqs. (5.4), (5.6), and (5.9) for $\varphi = 0.5$ and $S = 0.25$. (a) and (d) $\mathcal{F}$ (thick curves) and c_{LW} (thin curves) vs. a. (b) and (e) χ (thick curves) and $1 - a - \chi$ (thin curves) vs. a. (c) and (f) $\dot{\mathcal{D}}$ vs. a. The top and bottom rows show the mode 1 and mode 2 solutions, respectively. In all cases dashed and solid curves show solutions corresponding, respectively, to $\dot{\mathcal{D}} < 0$ and $\dot{\mathcal{D}} \geq 0$.

Figure 3(b)). Unlike the irrotational flow above a solid obstacle, the encounter between the gravity current and the ambient generates a jump inside the control volume; the streamlines between sections AD and BC are no longer smooth as compared to the flow of Figure 3(a). The most perfection we can require after the replacement of the solid obstacle with the layer of dense fluid is that the far upstream and far downstream speeds remain unchanged, like in the perfect flow about the obstacle (Figure 3(a)).

Equation (5.9) can be used to estimate the behavior of a physical gravity current when $a \ll 0$. The obvious requirement is that, in spite of the $O(a^{-1})$ coefficient, $\dot{\mathcal{D}}$ remains finite, of the order of unity, in the limit $a \to 0$. The very thin gravity current produces a small deviation of the thick ambient above, and hence $\chi = \varphi - O(a)$ (the minus sign reminds us that a decrease of value will occur). To maintain a finite $\dot{\mathcal{D}}$, it is necessary that

$$\mathcal{F} = [2(1 - S)]^{1/2} - O(a) \quad (a \ll 1). \tag{5.10}$$

Below, we confirm that Eq. (5.10) is a quite accurate prediction in the appropriate limit.

The rate of energy dissipation, $\dot{\mathcal{D}}$, is associated with a pressure head loss, Δ. Let Q be a point on the surface $z = h$ in the downstream domain outside the control volume. For ideal flow over the semi-infinite obstacle of Figure 3(a), the pressure at this point is given by Bernoulli's equation $P_{Qi} = \frac{1}{2}\rho_1(U^2 - u_1^2 - 2gh) + C$, where i denotes "ideal." In the slug-like gravity current, the pressure at this point is given by the hydrostatic relation $P_Q = P_O - \rho_c gh = \frac{1}{2}\rho_1 U^2 + C - \rho_c gh$. The difference between P_{Qi} and P_Q, scaled with $\rho_2 g'$ gives a (dimensional) head loss

$$\Delta = \frac{P_{Qi} - P_Q}{\rho_2 g'} = (1 - S)h - \frac{\rho_1 u_1^2}{2\rho_2 g'}. \tag{5.11}$$

Recall that in the Boussinesq case, $\rho_1/\rho_2 \approx 1$. Because the pressure above point Q is hydrostatic, and the speeds are the same as in the ideal case, the head loss result (5.11) applies at any vertical
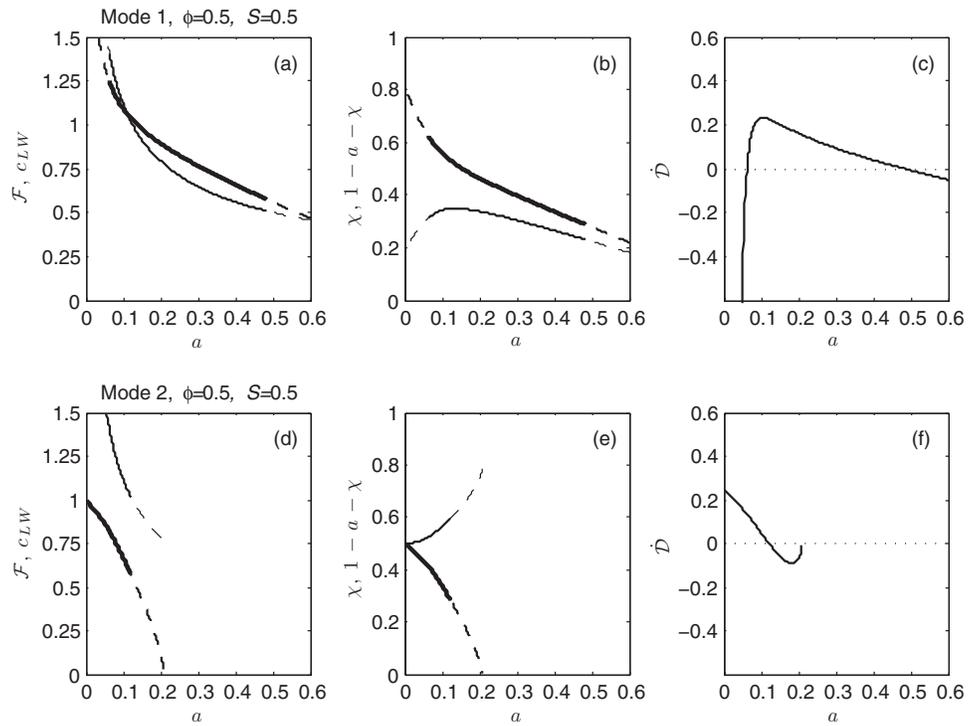
FIG. 5. As in Figure 4 but with $S = 0.5$.
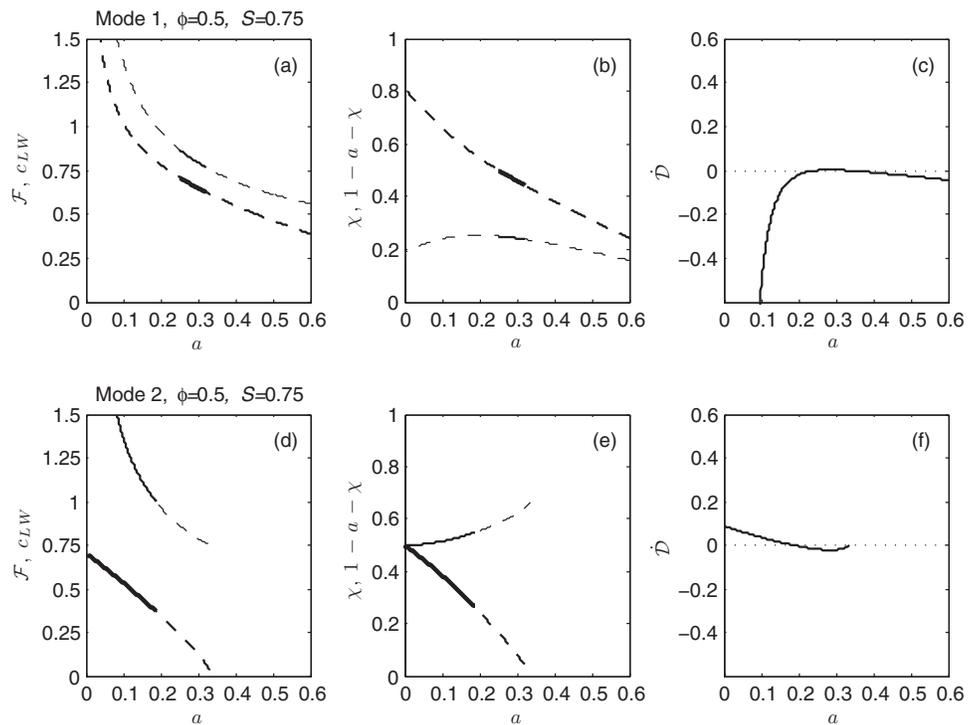
FIG. 6. As in Figure 4 but with $S = 0.75$.

position z satisfying $h \leq z \leq H$. In other words, the head loss is independent of elevation, like in Benjamin's solution.

It has been shown by Ungarish[11] that $\dot{\mathcal{D}}$ and Δ are related by

$$\Delta = \dot{\mathcal{D}}/(\rho_2 g' H U), \qquad (5.12)$$

where $\dot{\mathcal{D}}$ is dimensional. This equivalence applies here as well as can be verified by combining Eqs. (5.1) and (5.11), and then contrasting the result with Eq. (5.9). Furthermore, $\dot{\mathcal{D}} = 0$ corresponds to $\Delta = 0$, and for $a > a_{\max}$ or $a < a_{\min}$ we obtain the unphysical scenario $\Delta < 0$. However, Δ is, in general, an unreliable measure of dissipation because, according to Eq. (5.12), Δ is obtained by distributing the rate of dissipation $\dot{\mathcal{D}}$ over the entire height of the ambient, which may be large. Note that $\Delta/h = [\dot{\mathcal{D}}/(\rho_2 g' U h)]a$. For deep-ambient gravity currents (small a), Δ/h becomes a small number in spite of the fact that the term inside the brackets is of order unity, i.e., the physical dissipation does not decrease. A particularly problematic result is that the head loss vanishes as $a \to 0$. This may give the misleading conclusion that a very deep-ambient gravity current is energy-conserving.

A key difference between our analysis and that of Holyer and Huppert[8] is associated with the role attributed to energy dissipation. Holyer and Huppert[8] argued that energy dissipation fixes the value of a so that, in other words, a "second equation" (in addition to $U/(g'h)^{1/2} = \mathcal{F}$) can be formulated for the steady-state gravity current. More specifically, Holyer and Huppert[8] opined that the maximum dissipation for a certain throughput $M = Uh$ would occur, and that M would be maximized when not prescribed. They used Δ as a measure for energy dissipation, allowing for different values in the upper and lower layers of the ambient. In addition, Holyer and Huppert[8] attempted to impose reasonable values of the head loss and then calculate the reaction of the gravity current flow until the postulated maximum principles were realized. In these respects, and with the benefit of results that emerged following the publication of Holyer and Huppert's important study (e.g., as summarized in Ungarish[11]), the present analysis follows a rather different methodology. We argue that the precise value of h (or a) is determined by initial and boundary conditions. Steady-state gravity currents, like the one considered by Benjamin,[5] may emerge from various initial conditions; therefore, the steady-state solution must contain some degree of freedom that cannot be determined from time-independent considerations only. The most we can do with a pure steady-state gravity current problem, without adding adjustable constants, is to determine $\mathcal{F}$ as a function of a, subject to the condition that $\dot{\mathcal{D}} \geq 0$. In other words, if the variables U and h of the steady gravity current are unspecified, we are able to derive only one equation, not two. Moreover, Eq. (5.10) indicates that for a deep-ambient (small a) gravity current, the calculation of a from speed considerations is ill-conditioned.

A real gravity current, particularly the one issuing from a lock-release apparatus, is governed by hyperbolic equations with information carried along characteristics up- and downstream in the fluid of density ρ_c. In these cases $\mathcal{F}$ is a "jump condition" for speed as a function of h at the front where the characteristics encounter the unperturbed ambient. The "second equation" for speed as a function of h is provided by the information carried by the characteristics, not by dissipation considerations and the maximum volume flux of the gravity current, $M = Uh$. Our approach is fully consistent with Benjamin's solution and is predicated on the following observation:[11] for a more realistic gravity current, Benjamin's idealized $\mathcal{F}$ formula is a jump condition for the two-layer shallow-water equations of motion. Unique solutions for the dam-break problem are thereby obtained for both Boussinesq and non-Boussinesq gravity currents which propagate in a homogeneous ambient. In general, the lock-released gravity current does not attain maximum M; the exception is the critical (or choked) case when the characteristic speed matches that of the leading edge of the gravity current. This logic has been broadly applied to gravity currents and intrusions in homogeneous and linearly stratified ambients, for both the slumping and time-dependent stages of propagation, and has led to encouraging qualitative and quantitative agreements with observations in various circumstances.[4,9,20] It is therefore sensible to apply the same logic to the present problem. The theoretical advantage is that we derive a more general result, and the practical advantage is that we can use the similar simplified tools for the prediction of gravity currents in various related circumstances.

C. Results and comparisons with laboratory data

Sample solutions of steady-state gravity currents are shown in Figures 4–6, which consider $\varphi = 0.5$ and $S = 0.25, 0.5$, and 0.75, respectively. The Appendix shows analogous results when $\varphi > 0.5$ and $\varphi < 0.5$; similar trends are noted. In general, the solution is not unique for a given combination of parameters. Panels (a)–(c) show the mode 1 solution to Eqs. (5.4) and (5.6), whereas panels (d)–(f) consider the mode 2 solution. The middle panels of Figures 4–6 consider $\chi = h_{1L}/H$, which exhibits a monotonic variation with a, and $1 - a - \chi = h_{2L}/H$, which typically exhibits a non-monotonic variation, at least for the mode 1 solution. Panels (c) and (f) consider the variation of the dissipation rate $\dot{\mathcal{D}}$ with a and indicate that the physically acceptable $\dot{\mathcal{D}} \geq 0$ solution occurs over a restricted range of a, the breadth of which decreases (increases) with S for the mode 1 (mode 2) solution. When $\dot{\mathcal{D}} \geq 0$ ($\dot{\mathcal{D}} < 0$), the curves of panels (a), (b), (d), and (e) are indicated by the solid (dashed) lines corresponding to a physical (unphysical) flow.

For both the mode 1 and mode 2 solutions the behavior is consistent with Figure 3 of Ungarish[6] who considered a linearly stratified, rather than a two-layer, ambient. Thus, (i) $\mathcal{F}$ typically decreases with S and also with a; and (ii) the higher mode appears for small a and non-small S. Recall, however, that $a \ll 1$ is precisely the range in which Eq. (5.10) applies. Evaluation of Eq. (5.10) when $S = 0.25, 0.5$, and 0.75 shows that $\mathcal{F} = 1.225, 1$, and 0.7071, respectively. These values are in excellent agreement with the small a, mode 2 Froude numbers indicated, respectively, in Figures 4–6. Note moreover that the mode 1 front speed, $\mathcal{F}_1$, is a decreasing function of φ for fixed S whereas $\mathcal{F}_2$ is an increasing function of φ. For fixed φ, it is further observed that $\mathcal{F}_{1,2}$ typically decreases with S, although important exceptions arise, e.g., $\mathcal{F}_1$ for small a when $\varphi = 0.25$.

The stratified ambient is able to carry waves. As shown by Eq. (3.2.6) of Baines,[18] the speed of the dominant hydrostatic long wave, or characteristic, scaled with $(g'h)^{1/2}$, is

$$c_{LW} = \left[\frac{S\varphi(1-\varphi)}{a} \right]^{1/2}. \tag{5.13}$$

In contrast to the nomenclature applied in Tan $et\ al.$,[12] but consistent with the definition made by White and Helfrich,[7] a steady-state gravity current is said to be sub- or supercritical when $\mathcal{F} < c_{LW}$ or $\mathcal{F} > c_{LW}$, respectively. In each of Figures 4–6, we compare $\mathcal{F}$ (denoted by the thick curves of panels (a) and (d)) with c_{LW} (denoted by the thin curves of panels (a) and (d)). The mode 1 solution is typically supercritical (particularly for small S and non-vanishing a) whereas the mode 2 solution is universally subcritical. Combining Eqs. (5.10) with (5.13) we find the following sufficient condition for the subcriticality of a mode 2 deep-ambient gravity current:

$$S > \frac{2a}{\varphi(1-\varphi) + 2a} \quad (a \ll 1). \tag{5.14}$$

The interpretation of subcritical gravity currents poses difficulties. The fact that perturbations move faster than the gravity current gives rise to the question "What is the meaning of an "unperturbed ambient" on which the steady-state $\mathcal{F}$ was developed?"

The theoretical answer is that this is an imposed situation: we describe an analytically possible steady-state solution motion. This interpretation is a consistent extension of Benjamin's analysis in which the up- and downstream flows are given by simple solutions of the Euler equations, and we seek an eigenvalue (the dimensionless $\mathcal{F}$) that allows matching (without an energy source) while neglecting the initial and boundary conditions under which such a flow can be established and maintained.

In practical situations the answer is more complicated, particularly if we wish to draw a comparison between lock-released gravity currents (discussed in Sec. VI) and the steady-state prediction for $\mathcal{F}$. The gravity current released from behind a lock gate will inevitably excite transient perturbations. If the gravity current is subcritical (or even slightly supercritical with small φ), these perturbations may (and likely will) alter the initial conditions in the ambient fluid into which the gravity current propagates. Strictly speaking, this effect is incompatible with the assumptions made in the Benjamin-type control-volume balances used for the calculation of the steady-state $\mathcal{F}$. To proceed with the available solution, we must then rephrase the "unperturbed condition" postulate

as: we assume that the upstream perturbations cause only a minor alteration of the initial state. (Comparing theoretical predictions with experimental results, as we do in Figures 8–10, helps to clarify where this and other model assumptions are justified.)

A more rigorous alternative is to solve the coupled problem of the gravity current of unknown speed in an ambient with time-dependent stratification and layer-specific speeds. This is a formidable three-layer problem, and there is little hope that a reliable steady-state-speed solution, analytical or semi-analytical, can be obtained. The available guideline in this direction is, again, the solid-obstacle problem, as discussed in Sec. 3.6 of Baines[18] – see also Baines.[21] Thus, Figure 3.9 of Baines[18] indicates that an obstacle of sufficient height, suddenly introduced into a subcritical flow (or even a slightly supercritical flow with small φ) typically alters conditions upstream. (For reference, the parameters φ and $\mathcal{F}/c_{LW}$ in our analysis correspond to r and F_0 in Baines's figures; our a/φ resembles, qualitatively, his H_m.) As shown in Figure 3.14 of Baines,[18] such upstream effects are often manifested as a jump in the ambient interface that propagates ahead of the obstacle. The speed, magnitude, and strength of this jump depend on a variety of parameters; quantitative details are given in Baines's Figure 3.12. Unfortunately, these results do not carry over to the present problem: in contrast to the rigid topography, the gravity current is a deformable obstacle as exhibited experimentally, numerically, and schematically in Figures 2(a) and 2(c), 2(b) and 2(d), and 3(b), respectively (see also Figure 11(b) of the related investigation by White and Helfrich[7]). Correspondingly, the gravity current crest may represent a region of significant shear and vertical acceleration so that the hydraulic equations of motion cannot consistently be applied in this vicinity. As noted above, Benjamin's solution focuses on conditions far up- and downstream of the front and is not invalidated by such local vertical accelerations. The same cannot be said of Baines's solution, however, because the amplitude of the upstream-propagating disturbance "is controlled by a critical condition at the crest..." Finally, in the practical lock-release problem, the system is bounded by a vertical back wall which renders the shape of the "obstacle," and the boundary conditions different, in general, from those of the reported solutions. Of course, waves reflected in time-dependent lock-release problems may interact with the head of the gravity current, but this is a different effect.

Our understanding (based, admittedly, more on qualitative arguments than on rigorous analysis) is that the malleability and elongated shape of the gravity current will modify the alterations of the ambient stratification as compared to a solid obstacle of the same h in similar circumstances. It may then be the case that the effect of the upstream perturbation is, in general, different than would be expected from studies of flow over rigid topography. In this vein, and though less rigorous than the supercritical results, the subcritical solutions of $\mathcal{F}$ can still be considered as reasonable first approximations in a number of practical cases to be examined below. Where the agreement between theory and experiment proves unfavorable, an alternative approach pertinent to lock-released gravity currents and based on shallow-water theory is also available. The relevant derivation does not distinguish between sub- and supercritical gravity currents and is presented in Sec. VI.

Returning to Figures 4–6, recall that there are different intervals of a over which $\dot{\mathcal{D}} \geq 0$. On the basis of this observation, it is straightforward to evaluate $a_{\max}$ and $a_{\min}$ for various S; results are summarized graphically in Figure 7. The mode 1 solution can be realized only between the thick and thin solid curves; with $\varphi = 0.5$, Figure 7 predicts the mode 1 solution to be unphysical for all a when $S \gtrsim 0.754$ (cf. Figures 2 and 4 of Tan et al.[13]). Conversely, the mode 2 solution is anticipated only below the thick dashed curve.

Figure 7 predicts a thin region of bi-stability, in which the mode 1 and mode 2 solutions are simultaneously realizable; it corresponds to the area below the thick dashed curve but above the thin solid curve. By examining analogous results (not shown) corresponding to $\varphi = 0.25$ and $\varphi = 0.75$, we conclude that the area of this region of bi-stability increases with φ. In particular, for large φ, mode 2 solutions occur over a broader range of a. Although formal evidence is presently lacking, the mode 2 solution with its thicker and slower associated gravity current is, in our estimation, more likely to be realized in this region of bi-stability than the faster but thinner mode 1 solution. (Experiments are difficult to conduct in this regime principally because a is so small, however, there exists some support for this point of view – see, in particular, Figures 9(b) and 10(c).)
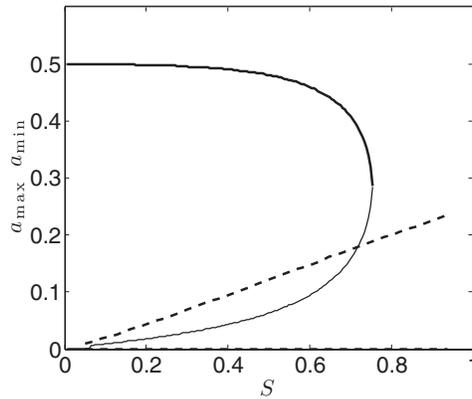
FIG. 7. $a_{\max}$ (thick curves) and $a_{\min}$ (thin curves) versus S for $\varphi = 0.5$. The mode 1 and mode 2 solutions are shown, respectively, by the solid and dashed lines. Note that $a_{\min}$ for mode 2 coincides with the horizontal axis.

In order to assess the steady-state results, we use the laboratory data that was obtained for lock-released gravity currents as described in Sec. II. There is evidence, presented in Sec. VI, that a lock-released gravity current experiences a quite significant slumping stage in which the speed of propagation, u_N, is constant and the domain behind the leading edge or nose is of constant height, h_N – the subscript N denotes the nose. (The determination of h_N is, of course, nontrivial in experiments or numerics because of billows and mixing. Because the situation is especially subjective when examining two-dimensional numerical output, examination of the Navier-Stokes simulations is deferred till Sec. VI B.) We therefore hope to find a correspondence between the measured data and the solution of the idealized steady-state gravity current with similar parameters, in particular, concerning the behavior of $\mathcal{F}$. Note, however, that this comparison cannot be regarded as an ironclad test of the steady-state theory: it is, in general, impossible to ascertain *a priori* the extent to which the assumptions of the theory are fulfilled in the intrinsically time-dependent lock-release flow. This uncertainty is increased when the real gravity current propagates with critical and subcritical $\mathcal{F}$.

Figures 8–10 indicate the variation of $\mathcal{F}$ with a for various S and φ. The solid and dashed curves are, respectively, the mode 1 and mode 2 theoretical results, and the circles indicate measurements derived from laboratory experiments. By contrast with theoretical predictions, the data points show a modest deviation of $\mathcal{F}$ with a and typically fall between $0.4 \leq \mathcal{F} \leq 0.6$ with larger
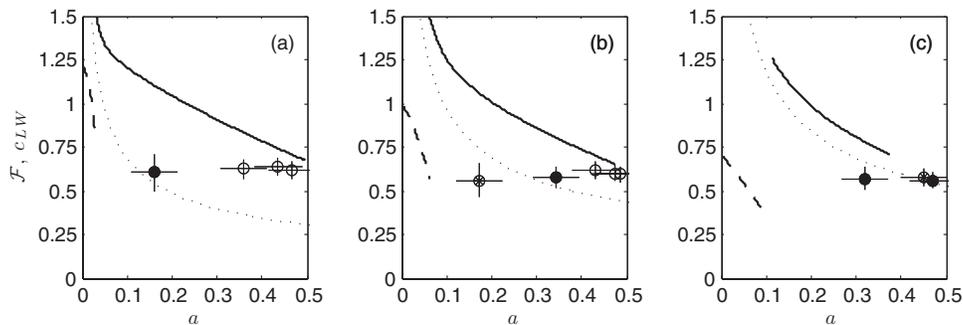

FIG. 8. $\mathcal{F}$ vs. a for $\varphi = 0.25$ and (a) $S = 0.25$, (b) $S = 0.5$, and (c) $S = 0.75$. The solid and dashed curves show the mode 1 and mode 2 front speeds, respectively. Laboratory measurements are indicated by the circles; closed and open symbols correspond, respectively, to instances in which an upstream-propagating disturbance was and was not observed. Open circles with a superimposed star correspond to in-between or indeterminate cases. The dotted curves show the non-dimensional long wave speed, c_{LW}.
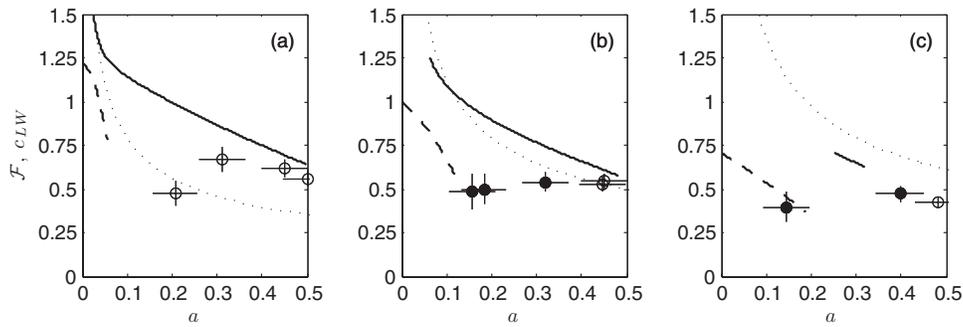
FIG. 9. As in Figure 8 but with $\varphi = 0.5$.

measured values occurring when φ and S are comparatively small in magnitude. In aggregate, the agreement between theory and experiment in Figures 8–10 can be considered to be fair with generally better correspondence arising for large φ and, more particularly, large a, i.e., the upper dissipation-free limit. White and Helfrich,[7] in their investigation of gravity current flow through an ambient with arbitrary stratification, refer to this dissipation-free limit as the "conjugate state." They likewise observe good agreement for large a but less favorable agreement for small a.

In addition to our previous comments concerning the difference between steady and time-dependent flows, there are numerous possible explanations for the offset observed in Figures 8–10. First, there are well-documented difficulties with measuring the gravity current height, particularly as this parameter approaches zero.[11] Because h_N is not a clear-cut defined variable, errors accumulate in both $a = h_N/H$ and $\mathcal{F} = u_N/(g'h_N)^{1/2}$. In the real flow, moreover, the speed may be z-dependent, while the theory assumes perfect z-independent moving cores of fluid. Furthermore, note that the most pronounced discrepancies when $S = 0.25$ occur for gravity currents with near-critical $\mathcal{F}$. In these cases, a gravity current started from rest into a given two-layer stratified ambient may attain such a speed in contrast with the ideal steady-state solution because of a head-wave interaction[3] that locks the speed of the gravity current to that of a (slower) interfacial wave.

There is, of course, the additional possibility of altered upstream conditions in which case the driving effect on the gravity current is expected to be diminished due to velocity perturbations and a displacement of the ambient interface. So as to carefully investigate this possibility, the experimental data points of Figures 8–10 distinguish between cases in which upstream-propagating disturbances were (closed circles) and were not (open circles) observed. Generally, though not universally, the closed and open data points fall below and above the dotted curves indicating the long wave
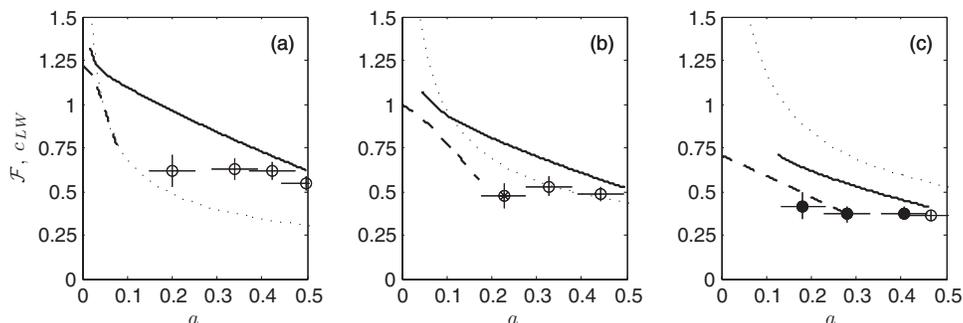
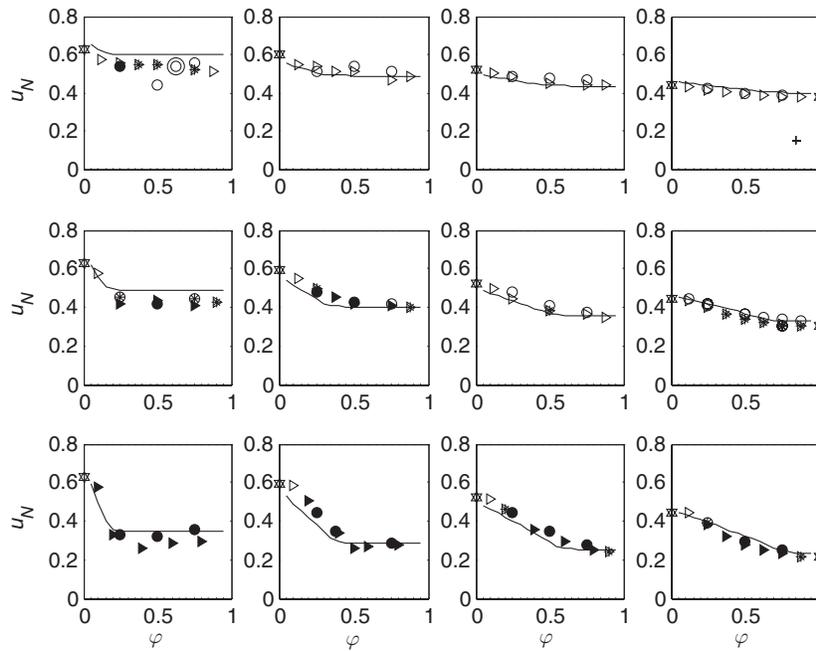FIG. 10. As in Figure 8 but with $\varphi = 0.75$.

FIG. 11. u_N vs. φ for $\Xi = 4.00$ (left column), $\Xi = 2.00$ (left-center column), $\Xi = 1.33$ (right-center column), $\Xi = 1$ (right column) and $S = 0.25$ (top row), $S = 0.5$ (middle row), $S = 0.75$ (bottom row). The solid lines indicate the analytical prediction of Sec. VI B. Experimental (circles) and numerical (right-facing triangles) data are also shown. Consistent with Figures 8–10, closed and open markers show, respectively, cases in which upstream-propagating disturbances were and were not observed; open markers with a superimposed star denote in-between or indeterminate cases. Six-pointed stars show experiments with $\varphi = 0$ or $\varphi = 1$ for which case the ambient is of uniform density. The "bull's eye" data point of the upper left panel denotes a high Reynolds number experiment, i.e., $\text{Re} = 11.3 \times 10^3$. By contrast, the left and right adjacent experimental data points have respective Reynolds numbers of $\text{Re} = 7.7 \times 10^3$ and $\text{Re} = 7.2 \times 10^3$. Representative error bars corresponding to the laboratory experiments are indicated in the upper right panel.

speed, c_{LW}. Closed data points arise with greater frequency when φ is small and S is large. From Figure 8(a), there is especially a poor agreement between the closed data point and the associated solid curve suggesting that upstream influences might be especially significant when $\varphi = S = 0.25$. On the other hand, similar discrepancies are noted in Figures 9(a) and 10(a) ($S = 0.25$) where no upstream-propagating disturbances were found. In instances where S is large, most notably in Figures 9(c) and 10(c), we observe much better agreement with the mode 1 and mode 2 branches of the theoretical solution. Although this is an area that demands future research, the above results suggest that upstream-propagating disturbances exert only a moderate influence in modifying the gravity current front speed during the slumping stage of propagation.

Note finally that a number of repeat experiments were performed employing identical S and geometric parameters (ambient interface height, depth of dense fluid in the lock, etc.) but with proportionally larger values for $\rho_c - \rho_2$ and $\rho_2 - \rho_1$. The variation in the scaled front speed was found to be within representative experimental uncertainty suggesting that Reynolds number effects, though an appealing culprit, are not responsible for the discrepancies documented in Figures 8–10. Further examination of Reynolds number effects can be found in our discussion of Figure 11.

From Figures 8–10 and with the benefit of the theoretical solutions for comparison, one can discern for select combinations of φ and S a shift from the mode 2 to the mode 1 solution. This transition is most evident in Figures 9(b) and 10(c). In the former case, we note that the experimental data points shift from the mode 1 solution to the mode 2 solution at larger values of a than those predicted theoretically. This could also have been anticipated: the speed of the lock-released gravity current develops with time from zero, and is influenced by viscosity. Consequently, the

gravity current will first appear as the slower mode 2 solution, and then require significant forcing for further acceleration to the faster mode 1 solution. Similar trends have been reported for gravity currents in a linearly stratified ambient.[22]

In other cases, notably when $S = 0.25$, it is unclear whether a transition from the mode 2 to the mode 1 solution does, in fact, occur. To take an extreme example, Figure 8(a) shows that the mode 2 solution exists only over a very limited range of a (i.e., for $a \lesssim 0.03$) when $\varphi = S = 0.25$. In this (and related) cases, the mode 2 solution may represent an "interesting feature of the steady solutions, [but not] a useful predictive tool."[7]

We conclude this section by placing Figures 8–10 into their proper context by making a comparison with Benjamin's classical solution. It, like the equations of Sec. V A, does not explicitly model a lock-release flow but rather considers the steady propagation of a gravity current (into a homogeneous ambient) without specific reference to lateral boundaries or initial conditions. In this simpler configuration, the typical discrepancy for $\mathcal{F}$ between theory and lock-release experiment is 30% for small a and about 25% for a close to 0.5 (this is, for example, the difference between Benjamin's results and those of Huppert and Simpson[23]). In aggregate, the agreement between theory and measurement exhibited in Figures 8–10 is of similar magnitude. Note, however, that generally larger discrepancies are noted for small a and small-to-moderate S. Wishing to address this region of parameter space and wishing also to provide a predictive tool of greater generality and reliability, it is worthwhile to consider, using the shallow-water equations, the time evolution of the lock-release flow. This is the subject of Sec. VI.

VI. SHALLOW-WATER THEORY

As noted above, a realistic gravity current, and, in particular, the widely studied lock-released flow depicted in Figure 2, are time-dependent phenomena subject to clear-cut initial and boundary conditions. The analysis of the idealized steady-state flow in the unbounded-x domain is relevant as a guiding line, but cannot model the observed motion as a function of x and t.

A simple model that is expected to close the gap between the steady-state solution and the more realistic flows of Figure 2 is the one-layer SW model. The major simplification comes from the assumption that there is no motion in either ambient layer. Consequently, the density and the hydrostatic pressure in layers 1 and 2 are like in the unperturbed state. The formal justification is that when the ambient is significantly thicker than the gravity current (i.e., for large Ξ where $\Xi \equiv H/h_0$) the return flow is weak, and the inertial forces in the ambient are negligible as compared to the hydrostatic driving.

Because the kinetic energy of the ambient is zero by definition, one-layer SW models do not always yield reliable predictions for the gravity current height, particularly as $\Xi \to 1$ in which case the canonical half-depth solution $a = \frac{1}{2}$ can be exceeded.[11] However, there is evidence concerning homogeneous and linearly stratified ambients[4, 24, 25] that these models are surprisingly robust when considering the front speed of the slumping stage even for values of Ξ down to 1. This auspicious record motivates the extension of the model to the stratification shown schematically in Figure 3(b).

A. Equations of motion

In this subsection, we again use the reduced pressure, defined so that $p = P + \rho_2 gz$ where $p_2 = 0$. The pressure in the unperturbed ambient is then

$$p_a(z) = \begin{cases} 0 & (h_{1R} < z \leq H) \\ (\rho_1 - \rho_2)g(h_{1R} - z) & (0 \leq z \leq h_{1R}) \end{cases}, \qquad (6.1)$$

and the pressure in the gravity current is

$$p_c(x, z, t) = -(\rho_c - \rho_2)gz + f(x, t). \qquad (6.2)$$

The condition of pressure continuity between p_a and p_c at $z = h$ determines the unknown function f. After some algebra, we obtain

$$p_c(x, z, t) = -(\rho_c - \rho_2)gz + (\rho_c - \rho_2)gh + p_a(h)\,. \tag{6.3}$$

The driving pressure gradient is therefore

$$\frac{\partial p_c}{\partial x}(x, t) = \begin{cases} \rho_2 g' \frac{\partial h}{\partial x} & (h > h_{1R}) \\ \rho_2 g'(1 - S)\frac{\partial h}{\partial x} & (h \leq h_{1R}) \end{cases}\,. \tag{6.4}$$

It is now appropriate to non-dimensionalize the variables. We scale horizontal lengths with the lock length x_0, heights with h_0, speeds with $(g'h_0)^{1/2}$, and time with $x_0/(g'h_0)^{1/2}$. The SW equations for $h(x, t)$ and $u(x, t)$ can now be derived by the same method as for the classical unstratified case.[11] (For both the stratified and unstratified cases, the continuity equation is the same.) In the z-averaged x-momentum equation, the stratification enters via the $\partial p_c/\partial x$ term given by Eq. (6.4). Consequently, in characteristic (and non-dimensional) form, the SW equations may be written as

$$\begin{bmatrix} h \\ u \end{bmatrix}_t + \begin{bmatrix} u & h \\ 1 - S\mathcal{H}(h) & u \end{bmatrix} \begin{bmatrix} h \\ u \end{bmatrix}_x = \begin{bmatrix} 0 \\ 0 \end{bmatrix}\,, \tag{6.5}$$

where $\mathcal{H}(h)$ is the unit step-function: $\mathcal{H}(h)$ has value 0 for $h > h_{1R}$, and value 1 for $h \leq h_{1R}$.

The system of equations given by Eq. (6.5) is hyperbolic in the parameter range of interest. Following the standard procedure, Eq. (6.5) yields the characteristic balances[11]

$$[1 - S\mathcal{H}(h)]^{1/2}\, h^{-1/2}\mathrm{d}h \pm \mathrm{d}u = 0\,, \tag{6.6}$$

on the characteristics

$$\frac{\mathrm{d}x}{\mathrm{d}t} = c_\pm = u \pm [1 - S\mathcal{H}(h)]^{1/2}\, h^{1/2}\,. \tag{6.7}$$

The initial conditions are zero velocity and unit dimensionless height and length at $t = 0$. For boundary conditions, we require zero velocity at $x = 0$ and apply a front condition at $x = x_N(t)$, which defines the nose of the gravity current.

B. Front condition

The front of the SW gravity current is a vertical shock produced by the intersection of the c_+ characteristics at the dam-break release. Taking a control volume about the jump (similar to the control volume $ABCD$ in Figure 3), and noting that the enclosed mass vanishes as the thickness of the control volume approaches zero, we conclude that the balances used in Sec. V to calculate $\mathcal{F}$ dominate the relationship between u_N and h_N. In other words, $u_N/h_N^{1/2}$ is a function of S, φ (or h_{1R} scaled with h_0 in the present formulation), and a (or h_N/Ξ in the present formulation). Formally, the previously derived rigorous values of $\mathcal{F}$ can be used. However, this possibility turns out to be awkward. The matching of the SW equations with the nose boundary condition entails iterations; in order to achieve smooth convergence, we require a relatively simple expression for $u_N/h_N^{1/2}$. Unfortunately, this description does not apply to the solutions of Sec. V, which were obtained using a process that leads to disparate mode 1 and mode 2 solutions. (In either case, no explicit analytical expression for $\mathcal{F}$ is available.) Moreover, a closer inspection shows that the steady-state equations and one-layer SW model are not entirely congruent because the latter discards the motion in the ambient. Therefore, the combination of the rigorous $\mathcal{F}$ with the present SW equations will inevitably contain approximation errors.

In view of these considerations, a more practical method is adopted. We develop a simplified form of $\mathcal{F}$ following, again, the methodology used for gravity currents in a linearly stratified ambient. While the exact steady-state balances of Ungarish[6] and White and Helfrich[7] yield complicated non-unique solutions for $\mathcal{F}$, Ungarish and Huppert[4] and Ungarish[9] used a much simpler approximation and still obtained SW solutions that agree well with experiments and simulations. The requisite approximation is based on the idea of separation of effects, which is itself suggested by Benjamin's solution (see Ungarish,[11] Secs. 3.2 and 12.2.1): the ratio of the dynamic reaction to the pressure

driving force on the front of the gravity current is a function of geometry (for both stratified and homogeneous ambients). Quantitatively and in dimensional form this separation of effects is expressed as

$$u_N = \text{Fr}(a) \times \left[\frac{P_c(z=0) - P_a(z=0)}{\rho_a} \right]^{1/2}. \tag{6.8}$$

Here, a is the depth ratio h_N/Ξ; P_c and P_a denote, respectively, the pressure of the gravity current and of the ambient; and ρ_a denotes the ambient fluid density and in the present Boussinesq case we take $\rho_a = \rho_2$. The advantages of Eq. (6.8) are: (i) the pressure term is straightforwardly given by Eqs. (6.1) and (6.3), and (ii) $\text{Fr}(a)$ can be taken "off the shelf" from the well-investigated case of flow into a homogeneous ambient. This evidence strongly suggests the use of the semi-empirical result usually referred to as the Froude number of Huppert and Simpson,[23]

$$\text{Fr}(a) = \text{Fr}_{HS}(a) = \begin{cases} 1.19 & (0 \le a \le 0.075) \\ 0.5 a^{-1/3} & (0.075 < a \le 1) \end{cases}. \tag{6.9}$$

We now combine Eq. (6.8) with Eqs. (6.1), (6.3), and (6.9) and scale the speed with $(g' h_0)^{1/2}$ and the height with h_0 and thereby obtain the following straightforward (non-dimensional) nose condition:

$$u_N = \begin{cases} \text{Fr}_{HS}(a) \left(1 - S \frac{h_{1R}}{h_N} \right)^{1/2} h_N^{1/2} & (h_{1R} < h_N) \\ \text{Fr}_{HS}(a)(1 - S)^{1/2} h_N^{1/2} & (h_N < h_{1R}) \end{cases}. \tag{6.10}$$

This front condition is simpler and more explicit than the implementation of the more rigorous steady-state $\mathcal{F}$. It is encouraging to note that for a deep-ambient gravity current the latter line of Eq. (6.10) is actually in good agreement with Eq. (5.10); the difference between the rigorous coefficient $2^{1/2}$ and the empirical 1.19 is a well-known effect. For additional justification, we subject the above results to comparisons with measured laboratory and numerical data in Sec. VI C.

C. Dam break and slumping

The initial propagation is of dam-break type, and the method of characteristics can be used to obtain an analytical solution of the SW equations, in particular, to determine the value of the speed of propagation.

Because $\mathcal{H}(h)$ is a simple function it is straightforward to integrate the characteristic balance equation (6.6). For a c_+ characteristic from the reservoir where $h = 1$, $u = 0$ to the nose where $h = h_N$, $u = u_N$ there are three alternatives:

1. $h_{1R} < h_N < 1$. The interface $h(x, t)$ separates fluid of density ρ_c below and fluid of density ρ_2 above; therefore $\mathcal{H}(h) = 0$ along the path of integration and

$$u_N = 2(1 - h_N^{1/2}). \tag{6.11}$$

2. $h_N < h_{1R} < 1$. The upper part of $h(x, t)$ resides in the domain of fluid 2, but the height of the gravity current decreases so that a part of it is covered by fluid of density ρ_1. In this case, $\mathcal{H}(h)$ is initially 0 then becomes 1 in the domain $h \le h_{1R}$, i.e.,

$$u_N = 2(1 - h_{1R}^{1/2}) + 2(1 - S)^{1/2}(h_{1R}^{1/2} - h_N^{1/2}). \tag{6.12}$$

3. $h_{1R} > 1$. The gravity current is now embedded in fluid of density ρ_1 from the beginning and correspondingly $\mathcal{H}(h) = 1$ on the path of integration. Therefore,

$$u_N = 2(1 - S)^{1/2}(1 - h_N^{1/2}). \tag{6.13}$$

The above results contain information provided by the conditions in the body of the dense fluid. This information must be combined with the jump condition (6.10) yielding two equations in the two unknowns h_N and u_N. Equations (6.11)–(6.13) are valid for all c_+ characteristics that emanate from the rectangular reservoir of stagnant dense fluid. Consequently, for some time interval following the lock-release, which we call the slumping time, h_N and u_N must remain constant. This prediction of the SW model nicely complements the present experimental observations in which a constant front speed is similarly observed (see also Figure 11 of Tan *et al.*[12]). The agreement represents a qualitative, but nevertheless important, corroboration of the SW model.

The next obvious step is the quantitative verification of the constant front speed. Here the simplified front condition (6.10) proves helpful. We found that the intersection of Eq. (6.10) with Eqs. (6.11)–(6.13) provides a well-converged and unique value of h_N. Subsequent substitution into Eq. (6.10) yields the analytical prediction of u_N. These results are shown as smooth curves in Figure 11, and comparisons with measured data (represented by the open and closed symbols of Figure 11) are now straightforward.

Consistent with White and Helfrich,[7] the overall impression from Figure 11 is of very satisfactory agreement over the entire (broad) range of tested parameters. Discrepancies are of the order of the measurement errors. We emphasize that the present analytical results were obtained from a well-defined set of general equations, without any adjustable constants or *ad hoc* closures. We used the semi-empirical Huppert-Simpson Fr formula, but this is a generic ingredient of numerous SW models,[11] not a special choice tailored to this particular problem.

A formally surprising outcome is that a favorable comparison between theory and experiment is obtained also for values of Ξ close to and equal to 1 ($\Xi = 1$ corresponding to a full-depth lock-release), whereas the one-layer SW model is expected to lose accuracy when there is a significant return flow in the ambient. We believe that this robustness demonstrates that the underlying physical mechanisms are well captured by the simplified equations. Although there certainly are approximation errors in the SW equations (6.5) and in the front condition (6.10), there is an internal cancellation that renders accurate values of the combined result u_N. We also note that the present solutions for the full-depth lock-release case are consistent with those of Tan *et al.*;[12] the present results, however, have the advantage of generality, while their solution pertains only to $\Xi = 1$.

Figure 11 shows that the speed of propagation decreases with S and φ. This is expected: by increasing either of S or φ, we increase the depth-averaged density of the ambient. Thus, the (dense) gravity current feels a smaller density difference, and hence a reduced buoyancy driving force. Even so, Figure 11 shows the following interesting effect: for a given S, u_N first decreases with φ, then attains a constant "plateau" for φ larger than some critical value. The interpretation is as follows. When φ increases from 0, the lower ambient layer thickens, and the overall density difference felt by the head of the gravity current is reduced. The maximum reduction is attained when $\varphi H = h_N$; further increase of φ will have a comparatively minor effect on the buoyancy driving force. We note again that the SW model captures well the behavior of the real gravity current.

The normalized speed of propagation increases with the depth-ratio parameter Ξ. This effect is well-documented from the classical homogeneous-ambient configurations.[11] A deep-ambient gravity current creates less return flow and hence encounters a smaller dynamic loss of driving force. Ambient stratification does not affect this trend.

The results displayed in Figure 11 cover scenarios in which upstream-propagating disturbances were and were not excited. When Ξ and S are small, there is, as expected, a reduced likelihood that such disturbances will occur. Even when they do occur, however, Figure 11 indicates that there is no marked deviation from the trend of the analytical solutions. We speculate that the influence of upstream-propagating disturbances will become significant at a later stage of motion, i.e., by dictating the point at which the gravity current begins to decelerate.[12, 14]

In summary, the comparisons discussed above provide strong support for the claim that the one-layer SW model developed in this paper, though dramatically simplified, captures well the leading-order dynamics of the flows exhibited in Figure 2 insofar as it provides accurate estimates of the front speed for a wide range of dimensionless parameters. This conjecture is consistent with the discussion of Ungarish and Huppert[4] who suggested that a decomposition of the type advocated

by Eq. (6.8) "reflects a local, quasi-steady integral property of the current head [that] is expected to remain valid also for a stratified ambient." Moreover, concerning the dynamic influence of waves in the ambient fluid, it has been concluded by Ungarish and Huppert,[4] Flynn and Sutherland,[26] and Flynn and Linden[10] that gravity currents propagating in stratified media impart only a modest fraction of their kinetic energy to such waves.

VII. DISCUSSION AND CONCLUSIONS

We have investigated the propagation of a gravity current into a two-layer stratified ambient, under the assumption of a high-Reynolds number and Boussinesq flow field. Both the steady-state and the lock-release problem were examined. Our main attention was focused on the derivation of analytical-theoretical results, however, laboratory experiments and Navier-Stokes simulations were also performed, principally to assess the validity of our analysis.

The advantage and novelty of our study is as follows. First, we developed and solved the motion from first principles, without relying on adjustable constants or *ad hoc* closures. Second, we obtained consistent extensions to existing theories for the homogeneous and linearly stratified ambients (in particular, the classical solution of Benjamin[5] for the steady-state case, and the widely used one-layer shallow-water model for the lock-release problem). Third, we contrasted our analytical results with experimental and Navier-Stokes data. Our results are consistent with the previous solutions of Holyer and Huppert[8] and Tan *et al.*,[12] but are more rigorous, applicable to a wider range of parameters, and more exhaustively validated.

The steady-state solution of Sec. V is thorough, and the results are, in general, non-unique, with a fast mode 1 and slower mode 2 arising as physically acceptable solutions in Figures 4–6. We demonstrated that energy dissipation considerations play a rather passive role in excluding some solutions because their realization would require an internal energy source. In any case, the steady-state result is mostly of fundamental theoretical-academic importance: it provides insights and guiding lines, but the analysis yields one implicit relationship in two unknowns (gravity current front speed and thickness). The result is given by the combination of Eqs. (5.4) and (5.6); it lacks a known analytical solution and does not admit initial or boundary conditions. Moreover, Figures 8–10 indicate that the agreement with laboratory data is relatively poor when the gravity current is thin and/or the ambient is deep.

By contrast, the one-layer shallow-water model of Sec. VI which we developed for the time-dependent gravity current is less rigorous than the steady-state solution (for example, it ignores the kinetic energy of the ambient layers and also neglects the influence of propagation on stratification), but turns out to be a versatile and accurate solver for the much-studied lock-release problem. The predicted values for speed of propagation are straightforwardly obtained and show good agreement with measurements over the entire (wide) range of tested parameters (see Figure 11). Notwithstanding the apparent simplicity of the one-layer shallow-water model formulation, the underlying physics of the flow seem to be well-represented. Adding this model to the existing body of literature yields a versatile calculation tool for the prediction of gravity currents in homogeneous, two-layer stratified, and linearly stratified ambients. Taken together, we believe that the associated collection of studies, which dates at least as far back as the 1983 investigation of Rottman and Simpson,[27] enhances the reliability of the pertinent body of knowledge particularly insofar as the front speed is concerned.

Because we considered a Boussinesq system, our results developed for a bottom gravity current can be immediately applied to a surface-top gravity current (a mirror image of our problem), and to the upper half of a symmetric intrusion (the lower half is again a mirror image). The behavior of a non-symmetric intrusion is a topic that needs a separate investigation.

Feasible extensions of the present work are to study the flow beyond the slumping stage and also to examine the flow dynamics in a cylindrical geometry. Viscous effects, which were neglected in the present investigation, are expected to become influential in these cases because of the decrease of speed and thickness with time. Either alternative requires nontrivial modifications of the Navier-Stokes numerical code and of the laboratory setup.

As noted above, a deficiency of our analytical solution is that it does not describe the effect of propagation on stratification. This effect may be significant in practical problems; the flow field around a propagating gravity current bears similarities (though also important differences as discussed above) to that over rigid topography; guidelines of the expected effect can be inferred from Baines,[18] in particular his Sec. 3.6. The more rigorous and quantitative investigation of the intriguing interaction between the three layers of fluid needs a dedicated study, and this must be left for future work.

ACKNOWLEDGMENTS

APPENDIX: FRONT CONDITION RESULTS FOR $\varphi \neq 0.5$

Figures 4 through 6 exhibit solutions to Eqs. (5.4), (5.6), (5.9), and (5.13) for various S but fixed φ, i.e. $\varphi = 0.5$. In Figures 12–17, we show analogous results for the cases $\varphi = 0.25$ and $\varphi = 0.75$. Similar trends are observed with the following notable exceptions: (i) when $\varphi = 0.25$ and $S \geq 0.5$, Figures 13 and 14 indicate that the mode 1 solution is universally supercritical; and (ii) when $\varphi = 0.75$ and $S = 0.25$, Figure 15 indicates that the mode 2 solution becomes supercritical, albeit briefly, i.e., for $0.048 \leq a \leq 0.071$.
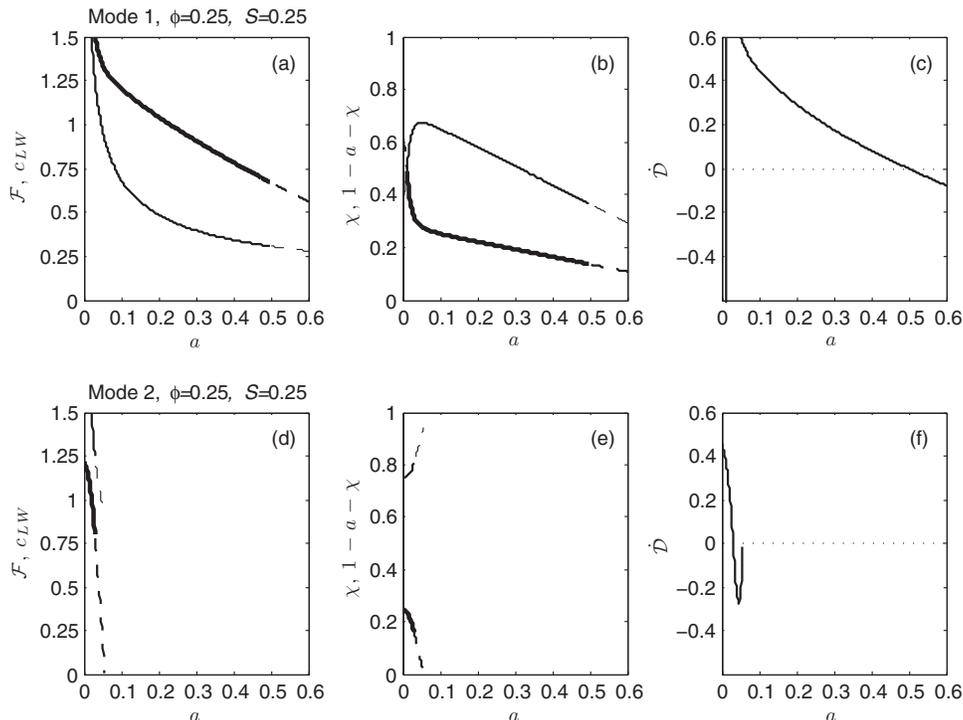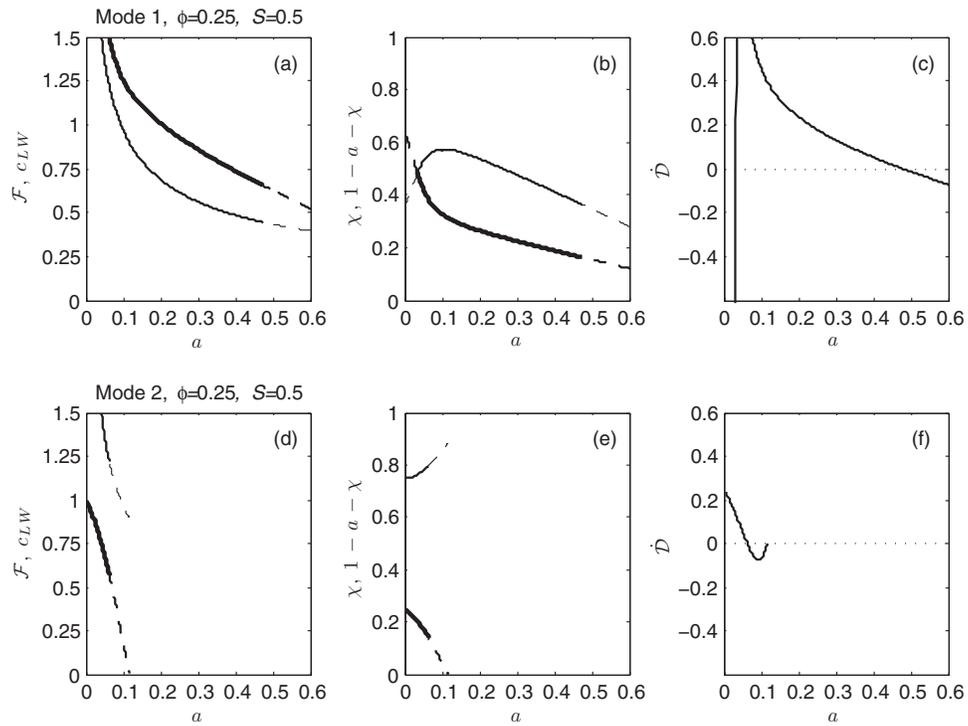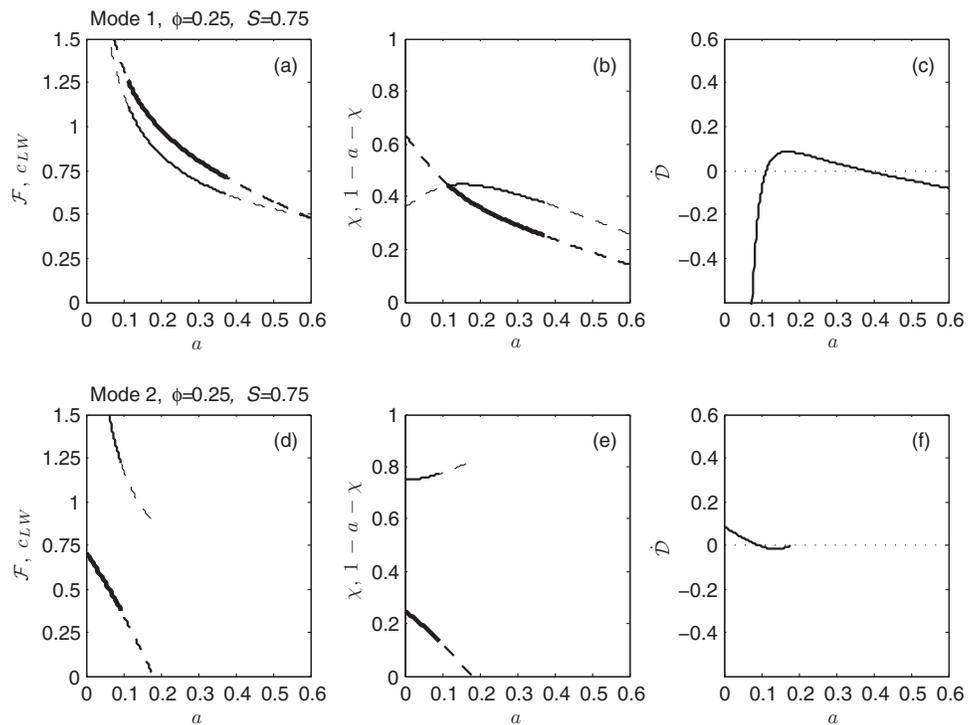

FIG. 12. As in Figure 4 but with $\varphi = 0.25$.

FIG. 13. As in Figure 5 but with $\varphi = 0.25$.

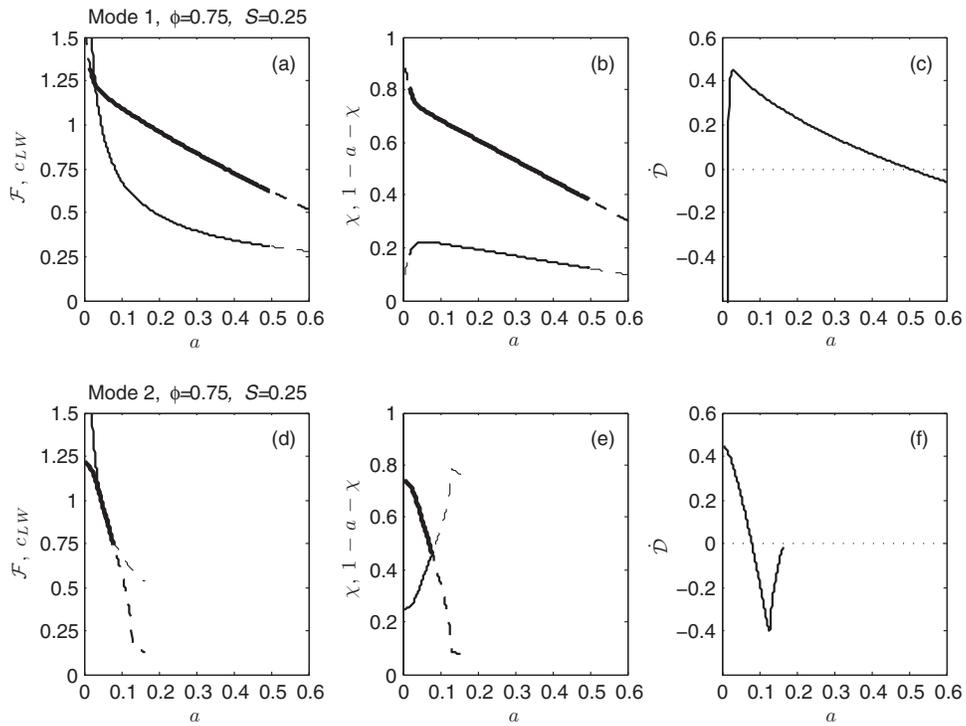FIG. 14. As in Figure 6 but with $\varphi = 0.25$.

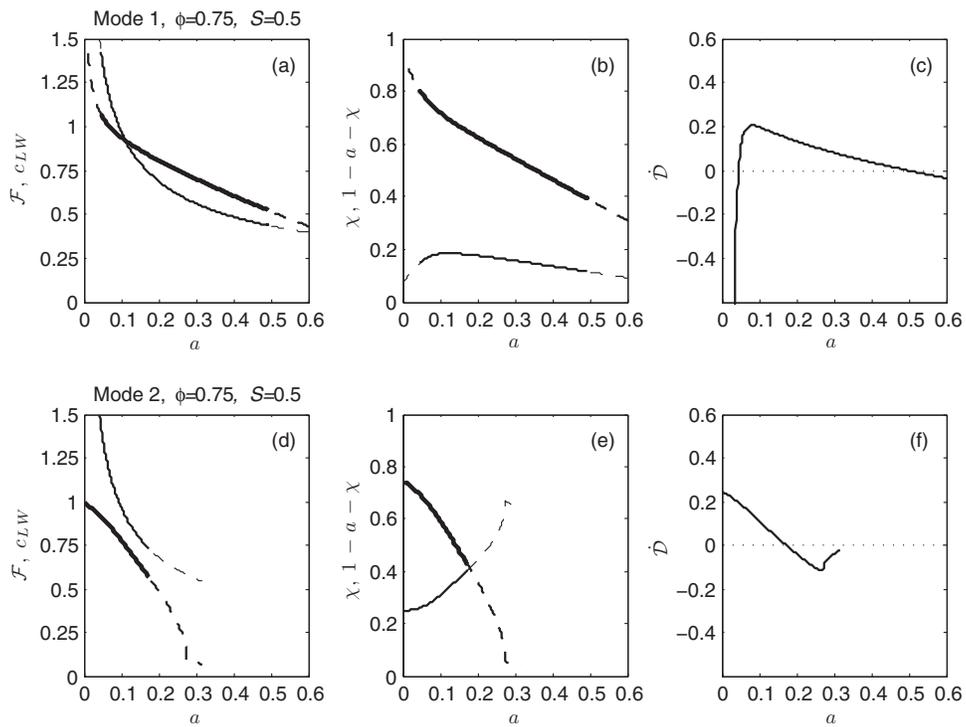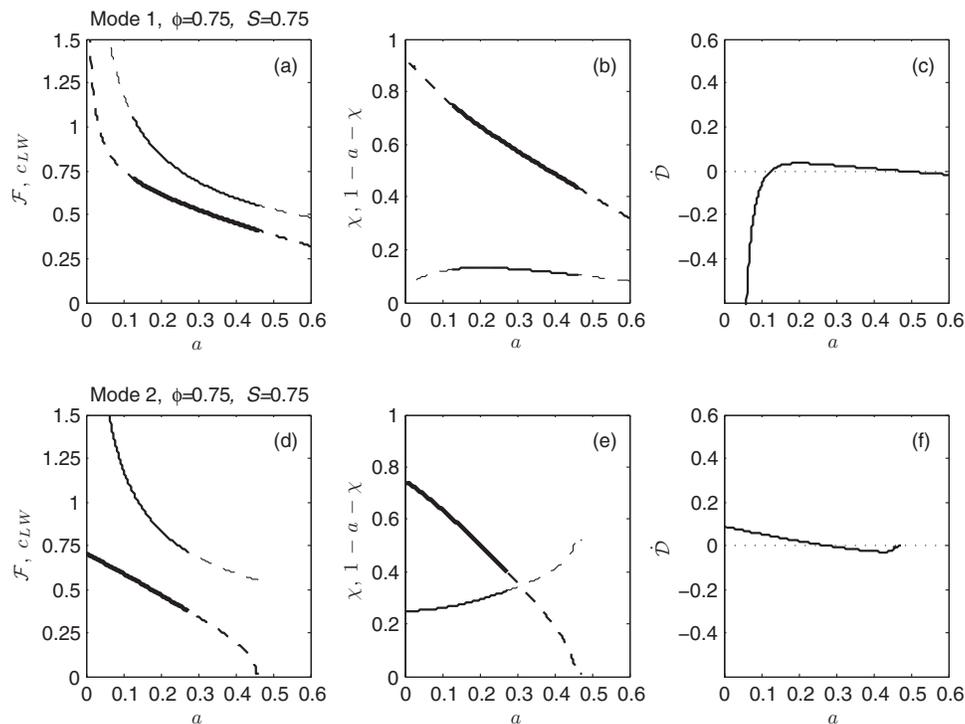FIG. 15. As in Figure 4 but with $\varphi = 0.75$.

FIG. 16. As in Figure 5 but with $\varphi = 0.75$.

FIG. 17. As in Figure 6 but with $\varphi = 0.75$.

[1] B. J. Devenish, G. G. Rooney, and D. J. Thomson, "Large-eddy simulation of a buoyant plume in uniform and stably stratified environments," J. Fluid Mech. **652**, 75 (2010).

[2] A. W. Woods, "Turbulent plumes in nature," Annu. Rev. Fluid Mech. **42**, 391 (2010).

[3] B. R. Sutherland and J. T. Nault, "Intrusive gravity currents propagating along thin and thick interfaces," J. Fluid Mech. **586**, 109 (2007).

[4] M. Ungarish and H. E. Huppert, "On gravity currents propagating at the base of a stratified fluid," J. Fluid Mech. **458**, 283 (2002).

[5] T. B. Benjamin, "Gravity currents and related phenomena," J. Fluid Mech. **31**, 209 (1968).

[6] M. Ungarish, "On gravity currents in a linearly stratified ambient: A generalization of Benjamin's steady-state propagation results," J. Fluid Mech. **548**, 49 (2006).

[7] B. L. White and K. R. Helfrich, "Gravity currents and internal waves in a stratified fluid," J. Fluid Mech. **616**, 327 (2008).

[8] J. Y. Holyer and H. E. Huppert, "Gravity currents entering a two-layer fluid," J. Fluid. Mech. **100**, 739 (1980).

[9] M. Ungarish, "Intrusive gravity currents in a stratified ambient – shallow-water theory and numerical results," J. Fluid Mech. **535**, 287 (2005).

[10] M. R. Flynn and P. F. Linden, "Intrusive gravity currents," J. Fluid Mech. **568**, 193 (2006).

[11] M. Ungarish, *An Introduction to Gravity Currents and Intrusions* (CRC, Boca Raton, FL, USA, 2009).

[12] A. W. Tan, D. S. Nobes, B. A. Fleck, and M. R. Flynn, "Gravity currents in two-layer stratified media," Environ. Fluid Mech. **11**(2), 203 (2011).

[13] A. W. Tan, D. S. Nobes, B. A. Fleck, and M. R. Flynn, "Gravity currents in two-layer stratified media," Environ. Fluid Mech. **11**(2), 225 (2011) (Erratum).

[14] A. W. Tan, "Gravity currents in two-layer stratified media," Master's thesis, University of Alberta, 2010.

[15] J. R. Taylor, "Numerical simulations of the stratified oceanic bottom boundary layer," Ph.D. dissertation (University of California, San Diego, 2008).

[16] C. Härtel, E. Meiburg, and F. Necker, "Analysis and direct numerical simulation of the flow at a gravity-current head. Part 1. Flow topology and front speed for slip and no-slip boundaries," J. Fluid Mech. **418**, 189 (2000).

[17] M. I. Cantero, J. R. Lee, S. Balachandar, and M. H. Garcia, "On the front velocity of gravity currents," J. Fluid Mech. **586**, 1 (2007).

[18] P. G. Baines, *Topographic Effects in Stratified Flows* (Cambridge University Press, Cambridge, England, 1995).

[19] M. Ungarish, "Energy balances for gravity currents with a jump at the interface produced by lock release," Acta Mech. **211**, 1 (2009).

[20] J. B. Klemp, R. Rotunno, and W. C. Skamarock, "On the dynamics of gravity currents in a channel," J. Fluid Mech. **269**, 169 (1994).

[21] P. G. Baines, "A unified description of two-layer flow over topography," J. Fluid Mech. **146**, 127 (1984).

[22] V. K. Birman, E. Meiburg, and M. Ungarish, "On gravity currents in stratified ambients," Phys. Fluids **19**, 086602 (2007).

[23] H. E. Huppert and J. E. Simpson, "The slumping of gravity currents," J. Fluid Mech. **99**, 785 (1980).

[24] M. Ungarish and T. Zemach, "On the slumping of high Reynolds number gravity currents in two-dimensional and axisymmetric configurations," Eur. J. Mech. B/Fluids **24**, 71 (2004).

[25] M. Ungarish, "A shallow-water model for high-Reynolds-number gravity currents for a wide range of density differences and fractional depths," J. Fluid Mech. **579**, 373 (2007).

[26] M. R. Flynn and B. R. Sutherland, "Intrusive gravity currents and internal gravity wave generation in stratified fluid," J. Fluid Mech. **514**, 355 (2004).

[27] J. W. Rottman and J. E. Simpson, "Gravity currents produced by instantaneous releases of a heavy fluid in a rectangular channel," J. Fluid Mech. **135**, 95 (1983).